Charged-particle transport in gases in electric and magnetic fields crossed at arbitrary angles: Multiterm solution of Boltzmann's equation

R. D. White,[1] K. F. Ness,[2] R. E. Robson,[1] and B. Li[1]
[1]*School of Computer Science, Mathematics and Physics, James Cook University, Cairns, Queensland 4870, Australia*
[2]*School of Computer Science, Mathematics and Physics, James Cook University, Townsville, Queensland 4811, Australia*
(Received 11 November 1998; revised manuscript received 31 March 1999)

A multiterm solution of the Boltzmann equation has been developed and used to calculate transport coefficients of charged-particle swarms in gases under the influence of electric and magnetic fields crossed at arbitrary angles ψ. The hierarchy resulting from a spherical harmonic decomposition of the Boltzmann equation in the hydrodynamic regime [Ness, Phys. Rev. A **47**, 327 (1993)] is solved numerically by representing the speed dependence of the phase-space distribution function in terms of an expansion in Sonine polynomials about a weighted sum of Maxwellian distributions at different temperatures. Results are given for charged-particle swarms in certain model gases over a range of ψ and field strengths. The variation of the transport coefficients with ψ is addressed using physical arguments. The errors associated with the two-term approximation and inadequacies of Legendre polynomial expansions are highlighted. [S1063-651X(99)12907-6]

PACS number(s): 52.25.Fi, 51.10.+y, 52.25.Dg, 51.60.+a

I. INTRODUCTION

The determination of transport properties of charged-particle swarms in gases under the influence of electric and magnetic fields crossed at arbitrary angles to each other is of interest not only from a theoretical viewpoint but has applications in many areas. In plasma processing, the magnetron discharge is an important device for deposition by sputtering [1]. Throughout the bulk plasma of the discharge the angle between the applied electric and magnetic fields varies. In high-energy physics, wire gas chamber detectors rely on the detection of electron swarms which result when the high-energy particles enter the gas chamber [2]. These detectors generally have various configurations of electric and magnetic fields applied to them (e.g., solenoidal and/or toroidal fields in the Atlas experiment), with specific requirements on the transport properties of the swarm needed to produce the desired spatial and temporal resolution for detection. The determination of low-energy charged particle–neutral particle cross sections via swarm experiments is a well established procedure [3]. In an attempt to improve accuracy and remove the lack of uniqueness in these cross sections, workers at Heidelberg developed swarm experiments in orthogonal electric and magnetic fields, and thus were able to exploit the extra dimension and degree of freedom introduced by virtue of the added magnetic field [4]. For arbitrary configurations of electric and magnetic fields, the degrees of freedom are further increased. Whether future generation swarm experiments could be designed to utilize these extra transport coefficients is yet to be determined. Other applications range from analysis of meteor trails [5] to high current switches [6]. The underlying requirement of the above applications is that further optimization of these technologies and experiments demand the most accurate modeling of charged particles in gases under the influence of arbitrarily configured electric and magnetic fields and a greater understanding of the physical processes that govern them. These represent the two principal themes of this paper.

The literature of theoretical investigations on charged-particle transport in electric and magnetic fields up to 1993 has been summarized in the papers by Ness [7] and Robson [8], with particular emphasis on orthogonal fields. We refer the reader to these papers for that configuration. For the more general case of arbitrary angles between the electric and magnetic field, understandably, there has been comparatively less investigation. In general Boltzmann equation treatments of this problem have been restricted to two-term Legendre polynomial expansions [9,10] and limited interaction models [11] and the associated limitations are well known. Biagi [12] extended the formulation of Huxley and Crompton [10] to a three-term theory and associated code MAGBOLTZ, though its limitations have been acknowledged and documented [7,13,14]. These limitations arise from incorrect symmetry assumptions in velocity space. These theories failed to acknowledge the work of Kelly [15], who earlier formulated a multiterm solution for arbitrary angles which avoided such assumptions. The treatment of transport in the presence of both density gradients and electric and magnetic fields was until 1993 by no means satisfactory. Although the anisotropic character of diffusion due to the magnetic field alone ($\boldsymbol{B}$ anisotropy) is well understood (see, e.g., Ref. [16]), the corresponding influence on the anisotropy introduced by the electric field ($\boldsymbol{E}$ anisotropy) was often ignored in discussions of transport in electric and magnetic fields [9,10] despite the experimental observations [17] and corresponding theoretical treatments [18]. Blum and Rolandi [19] addressed this ''double anisotropy'' theoretically through considerations of a series of rotation matrices. However, satisfactory systematic description encompassing both $\boldsymbol{E}$ and $\boldsymbol{B}$ anisotropies was not developed until Ness [7] did so. In the present work we demonstrate the influence of $\boldsymbol{E}$ anisotropy, $\boldsymbol{B}$ anisotropy, and anisotropy in velocity space (thermal anisotropy), and their couplings and discuss their resulting influence on the diffusion tensor.

 © 1999 The American Physical Society

Other theoretical and numerical techniques have also been applied to this problem. These include the semiquantitative momentum transfer theory using low order velocity moments of the Boltzmann equation [14,20] and Monte Carlo simulations [13]. Ikuta and Sugai [21] also applied their flight-time integral to the present problem, though the theoretical foundations and transport coefficient definitions of this theory have however come into question [22].

The aim of this paper is to present what we believe to be the first systematic solution of the Boltzmann equation for spatially inhomogeneous charged-particle swarms in gases under the influence of spatially uniform electric and magnetic fields crossed at arbitrary angles to each other. The starting point for this work is the hierarchy of kinetic equations derived by Ness [7], hereafter referred to as I. Aside from the assumption of central force interactions, the hierarchy has universal validity under hydrodynamic conditions and importantly is valid for charged particles of arbitrary mass, i.e., electrons through to heavy ions. We briefly review the general spherical harmonic decomposition of Ness [7] in Sec. II, before detailing the numerical technique employed to solve this hierarchy of kinetic equations. We introduce a slight modification to the traditional Sonine polynomial expansion which encompasses the two-temperature [15,23–25] and bi-Maxwellian [26] treatments. We pay particular attention to the symmetry properties of the Boltzmann equation and to the implications of these symmetries on the structure of tensors associated with the transport properties. In addition we comment on the structure and solution of the resulting hierarchy of moment equations. In Sec. III, the results of the multiterm solution and their physical interpretation are presented for light charge particle swarms in certain model gases. The reasons for using model cross sections in initial investigations are not always fully appreciated. The motivation is twofold.

(1) It is hoped that through the use of simple forms of cross sections we can isolate and elucidate fundamental physical processes which govern the variation of the transport coefficients and properties with various input parameters.

(2) Because of the analytic nature of the cross sections there is no uncertainty generated by the complicated structure of real cross sections, thus allowing for true quantitative comparisons of different theories and numerical techniques and the provision of benchmarks for future calculations and simulations.

It should be emphasized that this in no way restricts the applicability of the present theory or computer code. We defer the investigation of real gases to a future paper, preferring instead here to establish the validity of the theory and a qualitative understanding of the physics.

II. THEORY

The phase-space distribution function $f(\boldsymbol{r},\boldsymbol{c},t)$ for a dilute ensemble (or swarm) of charged particles moving through a neutral gas under the influence of electric and magnetic fields is described by the Boltzmann equation

$$\frac{\partial f}{\partial t}+\boldsymbol{c}\cdot\frac{\partial f}{\partial \boldsymbol{r}}+\frac{q}{m}[\boldsymbol{E}+\boldsymbol{c}\times\boldsymbol{B}]\cdot\frac{\partial f}{\partial \boldsymbol{c}}=-J(f,f_o), \tag{1}$$

where $\boldsymbol{r}$ and $\boldsymbol{c}$, respectively, denote the position and velocity coordinates; q and m, respectively, are the charge and mass of the swarm particle, and t is the time. The electric and magnetic fields are assumed to be spatially homogeneous and of magnitudes E and B, respectively. Swarm conditions are assumed to apply, and $J(f,f_o)$ denotes the rate of change of f due to binary particle-conserving collisions with the neutral molecules only. The neutral molecules of mass m_o are assumed to remain in thermal equilibrium at a temperature T_o. The original Boltzmann collision operator [27] and its semiclassical generalization [28] are used for elastic and inelastic processes respectively. No assumptions are made concerning the swarm particle to neutral molecule mass ratio. Nonconservative processes are left to a future paper. Throughout this paper we employ a coordinate system in which the z-axis is defined by $\boldsymbol{E}$ while $\boldsymbol{B}$ lies in the y-z plane, making an angle ψ with respect to $\boldsymbol{E}$.

A. Spherical-harmonic decomposition of the Boltzmann equation

The hierarchy of kinetic equations derived by Ness [7] has universal validity under hydrodynamic conditions, and forms the starting point for the present investigation. In review, the hierarchy was derived by representing the angular component of the velocity dependence of the phase-space distribution function in terms of an expansion in spherical harmonics:

$$f(\boldsymbol{r},\boldsymbol{c},t)=\sum_{l=0}^{\infty}\sum_{m=-l}^{l} f_m^{(l)}(\boldsymbol{r},c,t)Y_m^{[l]}(\hat{\boldsymbol{c}}), \tag{2}$$

where $Y_m^{[l]}(\hat{\boldsymbol{c}})$ are spherical harmonics, and $\hat{\boldsymbol{c}}$ denotes the angles of $\boldsymbol{c}$. Under hydrodynamic conditions a sufficient representation of the space dependence is an expansion in terms of powers of the density gradient operator [paper I, Eq. (17)]:

$$f_m^{(l)}(\boldsymbol{r},c,t)=\sum_{s=0}^{\infty}\sum_{\lambda=0}^{\infty}\sum_{\mu=-\lambda}^{\lambda} f(lm|s\lambda\mu;c)G_\mu^{(s\lambda)}n(\boldsymbol{r},t), \tag{3}$$

where the explicit expressions for the coefficients $f(lm|s\lambda\mu;c)$ are given by (I.18), $n(\boldsymbol{r},t)$ is the number density of charged particles and $G_\mu^{(s\lambda)}$ is the irreducible gradient tensor operator [39].

Substitution of Eqs. (2) and (3) into Eq. (1), premultiplying by $Y_m^{(l)}(\hat{\boldsymbol{c}})$ and integrating over all angles $\hat{\boldsymbol{c}}$ yields, on equating coefficients of $G_\mu^{(s\lambda)}n$, the following hierarchy of doubly-infinite coupled integro-differential equations [paper I, Eq. (24)]:

$$\sum_{l'=0}^{\infty}\sum_{m'=-l'}^{l'}\left[J^l\delta_{l'l}\delta_{m'm}-i\frac{qE}{m}(l'm10|lm)\langle l||\partial_c^{[1]}||l'\rangle\times\delta_{m'm}+\frac{qB}{m}\left\{\sqrt{(l-m)(l+m+1)}\frac{\sin\psi}{2}\delta_{m'm+1}-\sqrt{(l+m)(l-m+1)}\frac{\sin\psi}{2}\delta_{m'm-1}-im\cos\psi\delta_{m'm}\right\}\delta_{l'l}\right]f(l'm'|s\lambda\mu;c)=X(lm|s\lambda\mu), \tag{4}$$

where the individual expressions for the $X(lm|s\lambda\mu)$ are given by [paper I, Eq. (25)]. The reduced matrix elements J^l, $\langle l||\partial_c^{[1]}||l'\rangle$ and $\langle l||c^{[1]}||l'\rangle$ are given by Eqs. (18), (23), and (24), respectively, of Ref. [39]. The quantity $(l'm10|lm)$ denotes a Clebsch-Gordan coefficient. Solution of the hierarchy requires further treatment of the speed dependence of the phase-space distribution function, and this is considered in Sec. II B.

B. Solution of the hierarchy of kinetic equations

1. Expansion and symmetries

In this work the speed distribution function is expanded about a *single* distribution function $W(c)$ consisting of weighted sum of n Maxwellians each at a temperature T_b^i $(i=1,\ldots,n)$, in terms of modified Sonine polynomials $R_{\nu l}$:

$$f(lm|s\lambda\mu;c)=W(c)\sum_{\nu=0}^{\infty}F(\nu lm|s\lambda\mu;\alpha)R_{\nu l}(\alpha c), \quad (5)$$

where

$$W(c)=\sum_{i=1}^{n}b_i w(\alpha_i,c) \quad (6)$$

and b_i are real scalar weightings subject to the restriction

$$\sum_{i=1}^{n}b_i=1. \quad (7)$$

We also note that

$$w(\alpha_i,c)=\left(\frac{\alpha_i^2}{2\pi}\right)^{3/2}\exp\left\{\frac{-\alpha_i^2c^2}{2}\right\}, \quad (8)$$

$$\alpha_i^2=\frac{m}{kT_b^i}, \quad (9)$$

$$\alpha^2=\frac{m}{kT_b}, \quad (10)$$

$$R_{\nu l}(\alpha c)=N_{\nu l}\left(\frac{\alpha c}{\sqrt{2}}\right)^l S_{l+1/2}^{(\nu)}\left(\frac{\alpha^2c^2}{2}\right), \quad (11)$$

$$N_{\nu l}^2=\frac{2\pi^{2/3}\nu!}{\Gamma(\nu+l+3/2)}, \quad (12)$$

and $S_{l+1/2}^{(\nu)}(\alpha^2c^2/2)$ denote Sonine polynomials. This is an extension of the bi-Maxwellian treatment of Ness and Viehland [26]. The motivation for employing such a weighting function is discussed later. Normalization [paper I, Eq. (26)] requires

$$\sum_{i=1}^{n}b_i\sum_{\nu'=0}^{\infty}A_{0\nu'}^0(i)F(\nu'00|s\lambda\mu;\alpha)=\delta_{s0}\delta_{\lambda0}\delta_{\mu0}. \quad (13)$$

The modified Sonine polynomials at a basis temperature T_b are related to those at a basis temperature T_b^i via

$$R_{\nu l}(\alpha c)=\sum_{\nu_a=0}^{\nu}A_{\nu\nu_a}^l(i)R_{\nu_a l}(\alpha_i c), \quad (14)$$

where

$$A_{\nu\nu_a}^l(i)=\left(\frac{\nu}{\nu_a}\right)^2\frac{N_{\nu_a l}}{N_{\nu l}}\left(\frac{\alpha}{\alpha_i}\right)^{2\nu_a+l}\left[1-\left(\frac{\alpha}{\alpha_i}\right)^2\right]^{\nu-\nu_a}\frac{1}{(\nu-\nu_a)!}. \quad (15)$$

We note that, for $\nu_a>\nu$,

$$A_{\nu\nu_a}^l=0, \quad (16)$$

while if $T_b^i=T_b$ then

$$A_{\nu\nu_a}^l(i)=\delta_{\nu\nu_a}. \quad (17)$$

The following symmetry properties of the moments can be shown to exist:

$$F(\nu lm|s\lambda\mu;-\boldsymbol{E},\boldsymbol{B})=(-1)^{l+\lambda}F(\nu lm|s\lambda\mu;\boldsymbol{E},\boldsymbol{B}), \quad (18)$$

$$F(\nu lm|s\lambda\mu;\boldsymbol{E},-B_y,B_z)=(-1)^{m+\mu}F(\nu lm|s\lambda\mu;\boldsymbol{E},\boldsymbol{B}), \quad (19)$$

$$F(\nu lm|s\lambda\mu;\boldsymbol{E},B_y,-B_z)=(-1)^{m+\mu}F(\nu l-m|s\lambda-\mu;\boldsymbol{E},\boldsymbol{B}), \quad (20)$$

$$F(\nu lm|s\lambda\mu;\boldsymbol{E},-\boldsymbol{B})=F(\nu l-m|s\lambda-\mu;\boldsymbol{E},\boldsymbol{B}). \quad (21)$$

The implications of these symmetry properties on the transport coefficients will be discussed below.

For the specific configuration of *crossed fields*, it is evident from Eqs. (19) and (21) that condition (8c) of Ness [25] (hereafter referred to as II) is recovered:

$$F(\nu l-m|s\lambda-\mu)=(-1)^{m+\mu}F(\nu lm|s\lambda\mu). \quad (22)$$

For *parallel fields* it follows from Eqs. (20) and (21) that

$$m+\mu=\text{even}. \quad (23)$$

Furthermore, by considering the invariance under arbitrary rotations about the z axis, condition (23) is further strengthened to

$$m=\mu \quad (24)$$

for parallel fields and, hence,

$$F(\nu lm|s\lambda\mu)=0 \quad \text{if } m\neq\mu. \quad (25)$$

The reality of the phase-space distribution function implies

$$F^*(\nu lm|s\lambda\mu)=(-1)^{l+m+\lambda+\mu}F(\nu l-m|s\lambda-\mu), \quad (26)$$

where $*$ denotes complex conjugation. Thus in general the moments are complex. For crossed fields this reduces to

$$F^*(\nu lm|s\lambda\mu)=(-1)^{l+\lambda}F(\nu lm|s\lambda\mu), \quad (27)$$

through the use of Eq. (22). For this configuration, the moments are either purely real ($l+\lambda$ even) or purely imaginary ($l+\lambda$ odd). For parallel fields,

$$F^*(\nu lm|s\lambda\mu)=(-1)^{l+\lambda}F(\nu l-m|s\lambda-\mu)\quad(m=\mu) \tag{28}$$

and the moments are generally complex. The implications of the symmetry and reality considerations on the solution of the following hierarchy are considered below.

2. Hierarchy of moment equations

Substitution of Eq. (5) into Eq. (4), multiplying each member of the hierarchy by $R_{\nu l}(\alpha c)c^2$ and integrating over all speeds, yields through the use of the orthonormality of modified Sonine polynomials and Eq. (14), the following hierarchy of doubly infinite coupled algebraic equations for the moments:

$$\begin{aligned}
&\sum_{\nu'=0}^{\infty}\sum_{l'=0}^{\infty}\sum_{m'=-l'}^{l'}\left\{\sum_{i=1}^{n}b_i\sum_{\nu_a=0}^{\nu}A^{l}_{\nu\nu_a}(i)\right.\\
&\quad\times\sum_{\nu_b=0}^{\nu'}A^{l'}_{\nu'\nu_b}(i)\left[n_o J^{l}_{\nu_a\nu_b}(\alpha_i)\delta_{l'l}\delta_{m'm}\right.\\
&\quad+i\frac{qE}{m}\alpha_i(l'm10|lm)\langle\nu_a l||K^{[1]}(\alpha_i)||\nu_b l'\rangle\delta_{m'm}\\
&\quad+\frac{qB}{m}\left\{(\sqrt{(l-m)(l+m+1)}\,\delta_{m'm+1}\right.\\
&\quad-\sqrt{(l+m)(l-m+1)}\,\delta_{m'm-1})\left(\frac{\sin\psi}{2}\right)\\
&\quad\left.\left.-im\cos\psi\delta_{m'm}\right\}\delta_{\nu_a\nu_b}\delta_{l'l}\right]\Bigg\}F(\nu'l'm'|s\lambda\mu)\\
&\quad=X(\nu lm|s\lambda\mu),
\end{aligned} \tag{29}$$

where

$$X(\nu lm|000)=0, \tag{30}$$

$$\begin{aligned}
X(\nu lm|11\mu)=&\sum_{\nu'=0}^{\infty}\sum_{l'=0}^{\infty}\left[\sum_{i=1}^{n}b_i\sum_{\nu_a=0}^{\nu}A^{l}_{\nu\nu_a}(i)\right.\\
&\times\sum_{\nu_b=0}^{\nu'}A^{l'}_{\nu'\nu_b}(i)\left(-\frac{1}{\alpha_i}\right)(l'm-\mu1\mu|lm)\\
&\left.\times\langle\nu_a l||\alpha_i c^{[1]}||\nu_b l'\rangle F(\nu'l'm-\mu|000)\right]\\
&-\sum_{\nu'=0}^{\infty}\sum_{i=1}^{n}b_i\sum_{\nu_a=0}^{\nu}A^{l}_{\nu\nu_a}(i)A^{l}_{\nu'\nu_a}(i)\\
&\times\sum_{\nu_1=0}^{\infty}\sum_{j=1}^{n}b_jA^{1}_{\nu_1 0}(j)\frac{(-1)^{\mu}}{\alpha_j}\\
&\times F(\nu_1 1-\mu|000)F(\nu'lm|000),
\end{aligned} \tag{31}$$

and both ν and l range from 0 to ∞. The reduced matrix elements of the collision operator $J^{l}_{\nu\nu'}(\alpha_i)$, velocity $\langle\nu l||\alpha_i c^{[1]}(\alpha_i)||\nu'l'\rangle$ and velocity derivative $\langle\nu l||K^{[1]}(\alpha_i)||\nu'l'\rangle$ are given by Eqs. (11), (12a), and (12b), respectively, of Ref. [24]. The calculation of the matrix elements of the collision operator from interaction potentials is exceedingly difficult for all but the certain models. It is beyond the scope of this paper and we refer the reader to [29] for details. Note that only those expressions for the rhs which are required for the calculation of transport coefficients up to diffusion in the absence of nonconservative have been presented.

3. Truncation and convergence

The basis sets of modified Sonine polynomials and spherical harmonics together span velocity space and formally the combined expansions (2) and (5) should accurately represent the velocity distribution function, independent of the weighting function [here $\Sigma_i b_i w(\alpha_i,c)$]. Practically however, the upper limits on the ν and l summations must remain (manageably) finite at $\nu_{\max}$ and $l_{\max}$, respectively. Thus numerically, the phase-space distribution is approximated by

$$\begin{aligned}
f(\mathbf{r},\mathbf{c},t)\approx&\sum_{i=1}^{n}b_i w(\alpha_i,c)\sum_{s=0}^{1}\sum_{\lambda=0}^{s}\sum_{\mu=-\lambda}^{\lambda}\sum_{\nu=0}^{\nu_{\max}}\sum_{l=0}^{l_{\max}}\sum_{m=-l}^{l}\\
&\times F(\nu lm|s\lambda\mu)R_{\nu l}(\alpha c)Y^{[l]}_{m}(\hat{\mathbf{c}})G^{(s\lambda)}_{\mu}n(\mathbf{r},t).
\end{aligned} \tag{32}$$

The upper limits $\nu_{\max}$ and $l_{\max}$ are incremented individually until some convergence criterion on the transport coefficients and/or distribution function components are satisfied. Ness [25] referred to the m index as a pseudoindependent index, and showed that it can be truncated at some upper limit $m_{\max}$ ($0\leqslant m_{\max}\leqslant l_{\max}$) which is incremented until some convergence criterion is satisfied. This observation then allows the size of the coefficient matrix to be reduced.

The success of the above expansion is dependent on the choice of the weight function [30]. An unsuitable choice of weighting function often leads to a prohibitive number of terms required to achieve convergence and the scheme fails. Computationally it is more efficient to choose a weighting function which approximates the actual velocity distribution function as close as possible in some sense, thus minimizing the number of terms required in the expansions. (Depending on the collisional processes involved, the success of the scheme is dependent on representing certain parts of the distribution function better than others [31].) The motivation for the present weight function lies in the belief that with a suitable choice of the weightings and temperatures of these Maxwellians that the zeroth order approximation may be a close representation of the actual distribution. It is acknowledged that initially the algebraic complexity associated with such a weighting function is increased; however, we believe the associated added flexibility and the numerical efficiencies will more than compensate for the initial outlay of algebra. We also expect this code to have a wider range of applicability than that associated with the traditional two-temperature theory (see, e.g., Ref. [26]). For a single Maxwellian weighting function, there exist techniques for

estimating T_b, but the most effective method for electrons has been to leave it as a completely flexible parameter, used to optimize convergence. In the present scheme we leave all T_b^i and b_i as flexible parameters, and adjust them in a manner consistent with the physics of the problem.

4. Form and solution of the hierarchy

For conservative collisional processes, each member of the hierarchy is defined by the triplet (s,λ,μ), and has the following matrix form:

$$\mathbf{M}\boldsymbol{F}(s\lambda\mu)=\boldsymbol{X}(s\lambda\mu). \tag{33}$$

Elements of the matrix $\mathbf{M}$ are defined by the sextuplet (ν,ν',l,l',m,m'), and may be viewed as a matrix of matrices, exhibiting a block structure. Each block is defined by the quadruplet (l,l',m,m'), while individual elements within each block are defined by the pair (ν,ν'). Likewise, $\boldsymbol{F}$ and $\boldsymbol{X}$ may be viewed as a vector [defined by the pair (l,m)] of vectors (the individual elements of which are defined by the ν index).

We now examine the block structure of the coefficient matrix. The collision matrix and the matrix elements of the component of the magnetic field parallel to the electric field are both diagonal in both the l and m indices. The electric field terms are both subdiagonal and superdiagonal in the l indices, and diagonal in the m index. The matrix elements of the component of the magnetic field perpendicular to the electric field are diagonal in the l index but both subdiagonal and superdiagonal in the m index. Within each block, there exists certain structure within the ν indices. The elements of the electric field matrix blocks are diagonal in ν in the superdiagonal l blocks and superdiagonal in ν in the subdiagonal l blocks. All magnetic field matrix blocks are diagonal in the ν index. The elements of collision matrix blocks generally have no special properties (aside from certain model systems [29]).

Solution at any given level (s index), requires solutions of all lower members in the hierarchy. The order of solution of members (λ and μ indices) within any given level is arbitrary.

Condition (26) implies that in general for arbitrarily configured electric and magnetic fields the moments $F(\nu lm|s\lambda\mu)$ are *complex* and thus Eq. (29) represents a hierarchy of complex equations. It is only for the specific configuration of crossed fields that an appropriate transformation can be made so that all moments are real [viz.

$$\tilde{F}(\nu lm|s\lambda\mu)=i^{l+\lambda}F(\nu lm|s\lambda\mu), \tag{34}$$

which follows from Eq. (27)]. As it stands, a solution of hierarchy (29) will yield more information than is required for the evaluation of the transport coefficients and properties. Condition (26) provides relationships between moments with negative m or negative μ indices individually but not both simultaneously. This condition implies that we can (a) calculate the moments for all values of m and only non-negative values of μ, *or* (b) calculate the moments for all values of μ and only non-negative values of m. Both techniques yield all the required moments, so it is rather a matter of computational efficiency as to which is to be implemented. The first represents a tradeoff between increasing the size of the matrix to be inverted and decreasing the number of equations to be solved, while the latter represents a reduction in the size of the matrix to be inverted and an increase in the number of equations to be solved. Under the conservative conditions considered here, the coefficient matrix for each member of the hierarchy is unchanged, and only the right-hand-side vectors change. Thus it is anticipated that the first scheme will prove to more efficient. In the absence of reactions, the calculation of all transport coefficients up to diffusion, requires the solution of the following three members of the hierarchy: $(s,\lambda,\mu)=(0,0,0)$, $(1,1,1)$, and $(1,1,0)$.

In the absence of reactions, the first row of the coefficient matrix and the first element of the right-hand-side vector are zero for all members of the hierarchy. The first row of all matrix equations are then used to implement the normalization condition (13). The $(\nu,l,m)=(0,0,0)$ elements of $\mathbf{M}$ and $\boldsymbol{X}$ are then appropriately modified.

5. Transport coefficients and properties

The transport coefficients in this polynomial basis are given by

$$W_x=\sum_{\nu=0}^{\infty}\sum_{i=1}^{n} b_i A^1_{\nu 0}(i)\frac{1}{\alpha_i}\sqrt{2}\,\mathrm{Im}\{F(\nu 11|000)\}, \tag{35}$$

$$W_y=\sum_{\nu=0}^{\infty}\sum_{i=1}^{n} b_i A^1_{\nu 0}(i)\frac{1}{\alpha_i}\sqrt{2}\,\mathrm{Re}\{F(\nu 11|000)\}, \tag{36}$$

$$W_z=-\sum_{\nu=0}^{\infty}\sum_{i=1}^{n} b_i A^1_{\nu 0}(i)\frac{1}{\alpha_i}\mathrm{Im}\{F(\nu 10|000)\}, \tag{37}$$

$$D_{xx}=\sum_{\nu=0}^{\infty}\sum_{i=1}^{n} b_i A^1_{\nu 0}(i)\left\{-\frac{1}{\alpha_i}[\mathrm{Re}\{F(\nu 11|111)\}-\mathrm{Re}\{F(\nu 1-1|111)\}]\right\}, \tag{38}$$

$$D_{yy}=\sum_{\nu=0}^{\infty}\sum_{i=1}^{n} b_i A^1_{\nu 0}(i)\left\{-\frac{1}{\alpha_i}[\mathrm{Re}\{F(\nu 11|111)\}+\mathrm{Re}\{F(\nu 1-1|111)\}]\right\}, \tag{39}$$

TABLE I. Symmetry properties of the components of the drift velocity and diffusion tensor. The transformation represents A (parity), B (rotation of π about the z axis), C (parity and rotation of π about the y axis), and D (parity and rotation of π about the x axis).

	Transformation			
Coefficient	A	B	C	D
W_x	$W_x(-\boldsymbol{E},\boldsymbol{B})=-W_x(\boldsymbol{E},\boldsymbol{B})$	$W_x(\boldsymbol{E},-B_y,B_z)=-W_x(\boldsymbol{E},\boldsymbol{B})$	$W_x(\boldsymbol{E},B_y,-B_z)=W_x(\boldsymbol{E},\boldsymbol{B})$	$W_x(\boldsymbol{E},-\boldsymbol{B})=-W_x(\boldsymbol{E},\boldsymbol{B})$
W_y	$W_y(-\boldsymbol{E},\boldsymbol{B})=-W_y(\boldsymbol{E},\boldsymbol{B})$	$W_y(\boldsymbol{E},-B_y,B_z)=-W_y(\boldsymbol{E},\boldsymbol{B})$	$W_y(\boldsymbol{E},B_y,-B_z)=-W_y(\boldsymbol{E},\boldsymbol{B})$	$W_y(\boldsymbol{E},-\boldsymbol{B})=W_y(\boldsymbol{E},\boldsymbol{B})$
W_z	$W_z(-\boldsymbol{E},\boldsymbol{B})=-W_z(\boldsymbol{E},\boldsymbol{B})$	$W_z(\boldsymbol{E},-B_y,B_z)=W_z(\boldsymbol{E},\boldsymbol{B})$	$W_z(\boldsymbol{E},B_y,-B_z)=W_z(\boldsymbol{E},\boldsymbol{B})$	$W_z(\boldsymbol{E},-\boldsymbol{B})=W_z(\boldsymbol{E},\boldsymbol{B})$
D_{ii}	$D_{ii}(-\boldsymbol{E},\boldsymbol{B})=D_{ii}(\boldsymbol{E},\boldsymbol{B})$	$D_{ii}(\boldsymbol{E},-B_y,B_z)=D_{ii}(\boldsymbol{E},\boldsymbol{B})$	$D_{ii}(\boldsymbol{E},B_y,-B_z)=D_{ii}(\boldsymbol{E},\boldsymbol{B})$	$D_{ii}(\boldsymbol{E},-\boldsymbol{B})=D_{ii}(\boldsymbol{E},\boldsymbol{B})$
D_{xy}	$D_{xy}(-\boldsymbol{E},\boldsymbol{B})=D_{xy}(\boldsymbol{E},\boldsymbol{B})$	$D_{xy}(\boldsymbol{E},-B_y,B_z)=D_{xy}(\boldsymbol{E},\boldsymbol{B})$	$D_{xy}(\boldsymbol{E},B_y,-B_z)=-D_{xy}(\boldsymbol{E},\boldsymbol{B})$	$D_{xy}(\boldsymbol{E},-\boldsymbol{B})=-D_{xy}(\boldsymbol{E},\boldsymbol{B})$
D_{xz}	$D_{xz}(-\boldsymbol{E},\boldsymbol{B})=D_{xz}(\boldsymbol{E},\boldsymbol{B})$	$D_{xz}(\boldsymbol{E},-B_y,B_z)=-D_{xz}(\boldsymbol{E},\boldsymbol{B})$	$D_{xz}(\boldsymbol{E},B_y,-B_z)=D_{xz}(\boldsymbol{E},\boldsymbol{B})$	$D_{xz}(\boldsymbol{E},-\boldsymbol{B})=-D_{xz}(\boldsymbol{E},\boldsymbol{B})$
D_{yx}	$D_{yx}(-\boldsymbol{E},\boldsymbol{B})=D_{yx}(\boldsymbol{E},\boldsymbol{B})$	$D_{yx}(\boldsymbol{E},-B_y,B_z)=D_{yx}(\boldsymbol{E},\boldsymbol{B})$	$D_{yx}(\boldsymbol{E},B_y,-B_z)=-D_{yx}(\boldsymbol{E},\boldsymbol{B})$	$D_{yx}(\boldsymbol{E},-\boldsymbol{B})=-D_{yx}(\boldsymbol{E},\boldsymbol{B})$
D_{yz}	$D_{yz}(-\boldsymbol{E},\boldsymbol{B})=D_{yz}(\boldsymbol{E},\boldsymbol{B})$	$D_{yz}(\boldsymbol{E},-B_y,B_z)=-D_{yz}(\boldsymbol{E},\boldsymbol{B})$	$D_{yz}(\boldsymbol{E},B_y,-B_z)=-D_{yz}(\boldsymbol{E},\boldsymbol{B})$	$D_{yz}(\boldsymbol{E},-\boldsymbol{B})=D_{yz}(\boldsymbol{E},\boldsymbol{B})$
D_{zx}	$D_{zx}(-\boldsymbol{E},\boldsymbol{B})=D_{zx}(\boldsymbol{E},\boldsymbol{B})$	$D_{zx}(\boldsymbol{E},-B_y,B_z)=-D_{zx}(\boldsymbol{E},\boldsymbol{B})$	$D_{zx}(\boldsymbol{E},B_y,-B_z)=D_{zx}(\boldsymbol{E},\boldsymbol{B})$	$D_{zx}(\boldsymbol{E},-\boldsymbol{B})=-D_{zx}(\boldsymbol{E},\boldsymbol{B})$
D_{zy}	$D_{zy}(-\boldsymbol{E},\boldsymbol{B})=D_{zy}(\boldsymbol{E},\boldsymbol{B})$	$D_{zy}(\boldsymbol{E},-B_y,B_z)=-D_{zy}(\boldsymbol{E},\boldsymbol{B})$	$D_{zy}(\boldsymbol{E},B_y,-B_z)=-D_{zy}(\boldsymbol{E},\boldsymbol{B})$	$D_{zy}(\boldsymbol{E},-\boldsymbol{B})=D_{zy}(\boldsymbol{E},\boldsymbol{B})$

$$D_{zz}=\sum_{\nu=0}^{\infty}\sum_{i=1}^{n} b_i A^1_{\nu 0}(i)\left\{-\frac{1}{\alpha_i}F(\nu 10|110)\right\}. \tag{40}$$

Expressions for the off-diagonal elements of the diffusion tensor are not directly obtainable from the diffusion equation, but rather must be obtained from the flux-gradient expansion

$$n\langle \boldsymbol{c}\rangle = n\boldsymbol{W}-\mathbf{D}\cdot\boldsymbol{\nabla} n. \tag{41}$$

These components of the diffusion tensor are given by

$$D_{xy}=\sum_{\nu=0}^{\infty}\sum_{i=1}^{n} b_i A^1_{\nu 0}(i)\left\{-\frac{1}{\alpha_i}[\mathrm{Im}\{F(\nu 11|111)\}-\mathrm{Im}\{F(\nu 1-1|111)\}]\right\}, \tag{42}$$

$$D_{xz}=\sum_{\nu=0}^{\infty}\sum_{i=1}^{n} b_i A^1_{\nu 0}(i)\left\{\frac{\sqrt{2}}{\alpha_i}[\mathrm{Re}\{F(\nu 11|110)\}]\right\}, \tag{43}$$

$$D_{yx}=\sum_{\nu=0}^{\infty}\sum_{i=1}^{n} b_i A^1_{\nu 0}(i)\left\{\frac{1}{\alpha_i}[\mathrm{Im}\{F(\nu 11|111)\}+\mathrm{Im}\{F(\nu 1-1|111)\}]\right\}, \tag{44}$$

$$D_{yz}=\sum_{\nu=0}^{\infty}\sum_{i=1}^{n} b_i A^1_{\nu 0}(i)\left\{-\frac{\sqrt{2}}{\alpha_i}[\mathrm{Im}\{F(\nu 11|110)\}]\right\}, \tag{45}$$

$$D_{zx}=\sum_{\nu=0}^{\infty}\sum_{i=1}^{n} b_i A^1_{\nu 0}(i)\left\{\frac{\sqrt{2}}{\alpha_i}[\mathrm{Re}\{F(\nu 10|111)\}]\right\}, \tag{46}$$

$$D_{zy}=\sum_{\nu=0}^{\infty}\sum_{i=1}^{n} b_i A^1_{\nu 0}(i)\left\{\frac{\sqrt{2}}{\alpha_i}[\mathrm{Im}\{F(\nu 10|111)\}]\right\}. \tag{47}$$

Using the symmetry properties of the moments $F(\nu lm|s\lambda\mu)$ discussed in Sec. II B 1, the corresponding symmetry properties of the transport coefficients are detailed in Table I. The equivalent symmetry properties can be obtained without recourse to irreducible tensors. In the general case both the drift velocity vector and the diffusion tensor are *full*. Applying the symmetries in Table I, we observe that for parallel fields the drift velocity vector and diffusion tensor must have the following forms:

$$\boldsymbol{W}=\begin{pmatrix}0\\0\\W_z\end{pmatrix},\quad \mathbf{D}=\begin{pmatrix}D_{xx}&D_{xy}&0\\-D_{xy}&D_{xx}&0\\0&0&D_{zz}\end{pmatrix}, \tag{48}$$

while for orthogonal fields they reduce to the well known forms [8,25]

$$\boldsymbol{W}=\begin{pmatrix} W_x \\ 0 \\ W_z \end{pmatrix}, \quad \mathbf{D}=\begin{pmatrix} D_{xx} & 0 & D_{xz} \\ 0 & D_{yy} & 0 \\ D_{zx} & 0 & D_{zz} \end{pmatrix}. \tag{49}$$

These symmetry arguments can be extended to any of the transport properties of the same tensorial rank discussed below.

The average energy $\boldsymbol{\epsilon}(\boldsymbol{r},t)$ plays an important role in understanding various phenomena associated with drift and diffusion coefficients. In particular we utilize ε (spatially homogeneous mean energy) and γ (gradient energy parameter [32]), defined through a density gradient expansion of the average energy:

$$\boldsymbol{\epsilon}(\boldsymbol{r},t)=\frac{1}{n(\boldsymbol{r},t)}\int \frac{1}{2}mc^2 f(\boldsymbol{r},\boldsymbol{c},t)d\boldsymbol{c}=\varepsilon+\boldsymbol{\gamma}\cdot\frac{\nabla n}{n}+\cdots. \tag{50}$$

In the current representation, these quantities are given by

$$\varepsilon=\frac{3}{2}kT_b\sum_{\nu=0}^{\infty}\sum_{i=1}^{n} b_i\left[A^0_{\nu 0}(i)-\sqrt{\frac{2}{3}}\sum_{\nu_a=0}^{\nu}A^0_{\nu\nu_a}A^0_{1\nu_a}(i)\right]F(\nu 00|000), \tag{51}$$

$$\gamma_x=\frac{3}{2}kT_b\sum_{\nu=0}^{\infty}\sum_{i=1}^{n} b_i\left[A^0_{\nu 0}(i)-\sqrt{\frac{2}{3}}\sum_{\nu_a=0}^{\nu}A^0_{\nu\nu_a}A^0_{1\nu_a}(i)\right]\{-\sqrt{2}\,\mathrm{Im}\{F(\nu 00|111)\}\}, \tag{52}$$

$$\gamma_y=\frac{3}{2}kT_b\sum_{\nu=0}^{\infty}\sum_{i=1}^{n} b_i\left[A^0_{\nu 0}(i)-\sqrt{\frac{2}{3}}\sum_{\nu_a=0}^{\nu}A^0_{\nu\nu_a}A^0_{1\nu_a}(i)\right]\{\sqrt{2}\,\mathrm{Re}\{F(\nu 00|111)\}\}, \tag{53}$$

$$\gamma_z=\frac{3}{2}kT_b\sum_{\nu=0}^{\infty}\sum_{i=1}^{n} b_i\left[A^0_{\nu 0}(i)-\sqrt{\frac{2}{3}}\sum_{\nu_a=0}^{\nu}A^0_{\nu\nu_a}A^0_{1\nu_a}(i)\right]\mathrm{Im}\{F(\nu 00|110)\}. \tag{54}$$

The temperature tensor is defined in the usual manner

$$k\mathbf{T}=m\langle(\boldsymbol{c}-\langle\boldsymbol{c}\rangle)(\boldsymbol{c}-\langle\boldsymbol{c}\rangle)\rangle, \tag{55}$$

and is symmetric. To zeroth order in the density gradients, the diagonal elements of the temperature tensor are given by

$$T_{xx}=T_b\left[\sum_{\nu=0}^{\infty}\sum_{i=1}^{n} b_i\left\{\left[A^0_{\nu 0}(i)-\sqrt{\frac{2}{3}}\sum_{\nu_a=0}^{\nu}A^0_{\nu\nu_a}(i)A^0_{1\nu_a}(i)\right]F(\nu 00|000)\right.\right.$$
$$\left.\left.+A^2_{\nu 0}(i)\left[\sqrt{\frac{1}{3}}F(\nu 20|000)-\sqrt{2}\,\mathrm{Re}\{F(\nu 22|000)\}\right]\right\}-\left[\sum_{\nu=0}^{\infty}\sum_{i=1}^{n} b_iA^1_{\nu 0}(i)\sqrt{2}\mathrm{Im}\{F(\nu 11|000)\}\right]^2\right], \tag{56}$$

$$T_{yy}=T_b\left[\sum_{\nu=0}^{\infty}\sum_{i=1}^{n} b_i\left\{\left[A^0_{\nu 0}(i)-\sqrt{\frac{2}{3}}\sum_{\nu_a=0}^{\nu}A^0_{\nu\nu_a}(i)A^0_{1\nu_a}(i)\right]F(\nu 00|000)\right.\right.$$
$$\left.\left.+A^2_{\nu 0}(i)\left[\sqrt{\frac{1}{3}}F(\nu 20|000)+\sqrt{2}\,\mathrm{Re}\{F(\nu 22|000)\}\right]\right\}-\left[\sum_{\nu=0}^{\infty}\sum_{i=1}^{n} b_iA^1_{\nu 0}(i)\sqrt{2}\,\mathrm{Re}\{F(\nu 11|000)\}\right]^2\right], \tag{57}$$

$$T_{zz}=T_b\left[\sum_{\nu=0}^{\infty}\sum_{i=1}^{n} b_i\left\{\left[A^0_{\nu 0}(i)-\sqrt{\frac{2}{3}}\sum_{\nu_a=0}^{\nu}A^0_{\nu\nu_a}(i)A^0_{1\nu_a}(i)\right]F(\nu 00|000)-\frac{2}{\sqrt{3}}A^2_{\nu 0}(i)F(\nu 20|000)\right\}\right.$$
$$\left.-\left[\sum_{\nu=0}^{\infty}\sum_{i=1}^{n} b_iA^1_{\nu 0}(i)\mathrm{Im}\{F(\nu 10|000)\}\right]^2\right],$$

$$T_{xy}=T_b\left[\sum_{\nu=0}^{\infty}\sum_{i=1}^{n} b_i\{\sqrt{2}A^2_{\nu 0}(i)\mathrm{Im}\{F(\nu 22|000)\}\}-\left(\sum_{\nu=0}^{\infty}\sum_{i=1}^{n} b_iA^1_{\nu 0}(i)\sqrt{2}\,\mathrm{Im}\{F(\nu 11|000)\}\right)\right.$$
$$\left.\times\left(\sum_{\nu=0}^{\infty}\sum_{i=1}^{n} b_iA^1_{\nu 0}(i)\sqrt{2}\,\mathrm{Re}\{F(\nu 11|000)\}\right)\right], \tag{58}$$

$$T_{xz}=T_b\left[\sum_{\nu=0}^{\infty}\sum_{i=1}^{n} b_i\left\{\sum_{\nu_a=0}^{\nu}\sqrt{2}A^2_{\nu 0}(i)\,\mathrm{Re}\{F(\nu 21|000)\}\right\}-\left(\sum_{\nu=0}^{\infty}\sum_{i=1}^{n} b_i A^1_{\nu 0}(i)\sqrt{2}\,\mathrm{Im}\{F(\nu 11|000)\}\right)\right.$$
$$\left.\times\left(-\sum_{\nu=0}^{\infty}\sum_{i=1}^{n} b_i A^1_{\nu 0}(i)\,\mathrm{Im}\{F(\nu 10|000)\}\right)\right], \tag{59}$$

$$T_{yz}=T_b\left[\sum_{\nu=0}^{\infty}\sum_{i=1}^{n} b_i\left\{-\sum_{\nu_a=0}^{\nu}\sqrt{2}A^2_{\nu 0}(i)\,\mathrm{Im}\{F(\nu 21|000)\}\right\}-\left(\sum_{\nu=0}^{\infty}\sum_{i=1}^{n} b_i A^1_{\nu 0}(i)\sqrt{2}\,\mathrm{Re}\{F(\nu 11|000)\}\right)\right.$$
$$\left.\times\left(-\sum_{\nu=0}^{\infty}\sum_{i=1}^{n} b_i A^1_{\nu 0}(i)\,\mathrm{Im}\{F(\nu 10|000)\}\right)\right]. \tag{60}$$

This concludes the discussion on the theoretical formalism for the multiterm solution of the Boltzmann equation in the hydrodynamic regime in the presence of electric and magnetic fields at arbitrary angles to each other. We now apply this theory to a series of model gases to investigate the variation of the transport coefficients with the angle between the electric and magnetic fields.

III. RESULTS AND DISCUSSION

The aim of the present section is to highlight general features of the various transport properties and coefficients associated with the light ion swarms in gases in electric and magnetic fields. We defer details to the appendixes, where results are given and compared with established values, and prefer here to develop an appreciation for the physics associated with swarms in electric and magnetic fields at arbitrary angles ψ. We restrict our discussion and results to the influence of varying the angle between the electric and magnetic fields, and consider only a limited number of magnetic field strengths and fix the electric field. Discussion of the influence of the remaining permutations of E, B, and ψ will be left to a future paper. In the following sections we present results only for values of ψ between 0 and $\pi/2$. Extension to other angles can be made through use of symmetry properties in Table I. We adopt the unit of the huxley (Hx) for the reduced magnetic field B/n_o [25]: $1\,\mathrm{Hx}=10^{-27}\,\mathrm{Tm}^{-3}$.

In the following sections we often find it necessary to refer to the charged-particle trajectories to explain certain phenomena and the following elementary considerations apply: In the absence of collisions, charged particles in electric and magnetic fields gyrate about the magnetic field lines at a frequency $\Omega=qB/m$ with a Larmour radius $r=mc_T/qB$, where c_T is the tangential speed of the orbit. The guiding centers have a velocity $\boldsymbol{E}\times\boldsymbol{B}/B^2$. Superimposed on this picture is a component of the velocity in the $\boldsymbol{B}$ direction determined by the component of the electric field and the initial velocity of the charged particle in that direction. The influence of the collisions can be explained in terms of the ratio of the gyrofrequency Ω and the collision frequency ν. In the collision-dominated regime $\Omega\ll\nu$, the charged particles on average complete only partial orbits between collisions, while conversely in the field-dominated regime $\Omega\gg\nu$, the charged particles on average execute many gyrations per collision.

Throughout this section we employ two models: (i) the Maxwell model, where the collision frequency is independent of energy [see Eq. (A1) in Appendix A]; and (ii) the Reid ramp inelastic model [33] [see (B1) of Appendix B]. The utility of the Maxwell model lies in the fact that all variations are associated purely with the configuration and strengths of the electric and magnetic fields, and are not due to implicit variations associated with any dependence on the collision frequency upon energy. The Reid model will enable us to determine the influence of an energy dependent collision frequency in addition to the influence of strong inelastic processes. We highlight general features where appropriate. Model specific results will be highlighted and for the greater part will appear in the Appendixes.

A. Mean energy and drift speed

The mean energy monotonically decreases with ψ and/or B/n_o as in Fig. 1, and represents the phenomenon of magnetic cooling. This phenomenon is independent of the gas considered. The physical mechanism for the cooling action of a component of the magnetic field perpendicular to the electric field has been detailed previously [25,34]. The mechanism basically involves the perpendicular component of the magnetic field on the average turning the charged particles against the electric field. This reduces the ability of the electric field to pump energy into the swarm. This mechanism is enhanced as the component of the magnetic field perpendicular to the electric field (and hence ψ) is increased. For parallel fields, on average the electrons are traveling in the direction of the electric and magnetic field and hence the magnetic field has no explicit effect. Consequently the mean energy is independent of B/n_o. For this model, the drift speed is a one-to-one function of the mean energy, and hence the drift speed displays the same trends. This is a general rule, though there are exceptions, e.g., gases which give rise to negative differential conductivity.

B. Drift velocity components

The symmetry properties detailed in Sec. II are independent of the gas considered. In Fig. 2 these general symmetries are evident: $W_x=W_y=0$ for $\psi=0$, while $W_y=0$ for $\psi=90°$. The trends with ψ in these components viz., the magnitudes of W_x, W_y, and W_z monotonically increasing, having a maximal property and monotonically decreasing, re-

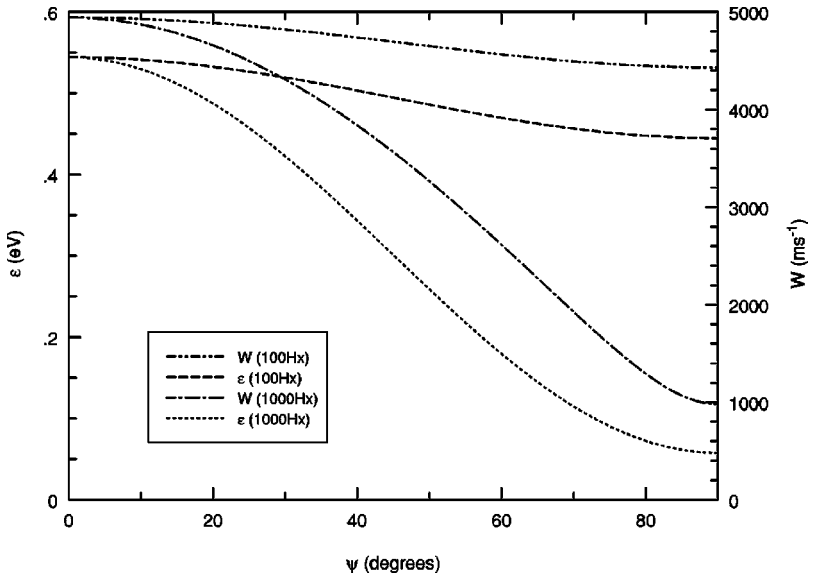

FIG. 1. Variation of the mean energy and drift speed as a function of ψ for the Maxwell model (A1).

spectively, are a consequence of the symmetry properties and are thus qualitatively general. The value of ψ for which the magnitude of W_y is a maximum is dependent on the gas considered. Consideration of profiles for additional B/n_o reveals that for a fixed ψ, the magnitudes of W_x, W_y, and W_z display respectively a maximal property, monotonically increase and monotonically decrease as B/n_o is increased. An interesting point to note is that the Lorentz angle (the angle the drift velocity vector makes with the electric field) monotonically increases with increasing ψ. For strong magnetic fields this angle approaches ψ [14]. These properties can be easily explained through consideration of the charged-particle orbits (see, e.g., Refs. [25,34]).

C. Diffusion tensor: triple anisotropy

Aside from the general symmetry properties outlined in Sec. II it is in general difficult to isolate features of the diffusion which are common to all electron or ion-neutral systems. This is in part due to the complexity of factors which contribute to or influence the diffusion tensor. Individually, these contributions/influences are (a) dispersion associated with different thermal random motion of the charged particles in different directions (thermal anisotropy); (b) explicit affects associated with the preferential orientation of orbitals of the charged particles in relation to $\boldsymbol{B}$ (magnetic anisotropy); and (c) spatial variation of ''local'' average velocities, labeled the ''differential velocity effect'' in relation to $\boldsymbol{E}$ (electric anisotropy) [32,35]. Moreover, the complexity is further increased by virtue of the couplings that arise between these contributions/influences, between (a) and (b) in addition to (b) and (c). These contributions and couplings can be understood from an examination of the following approximate expression, which is a generalization of that obtained in Ref. [35] to account for $\boldsymbol{B}$:

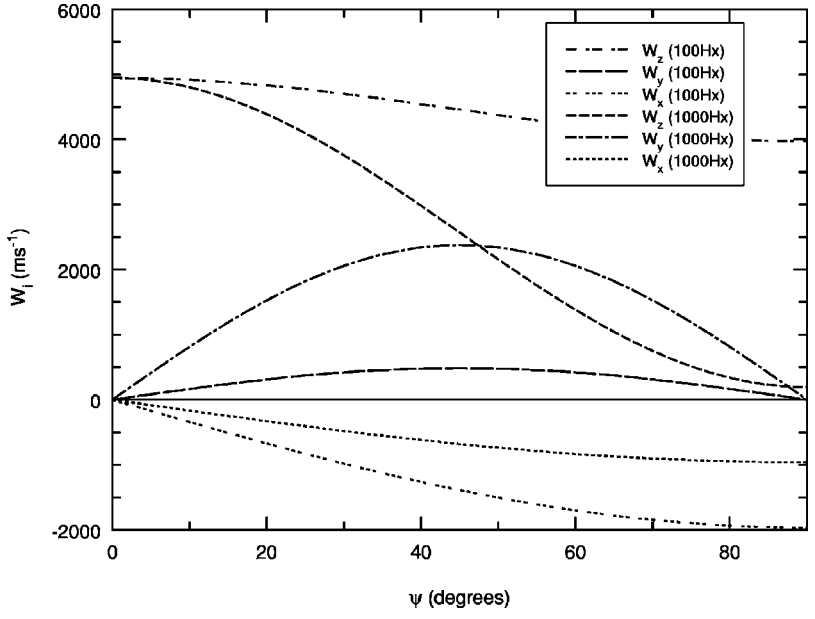

FIG. 2. Variation of the Cartesian drift velocity components as a function of ψ for the Maxwell model (A1).

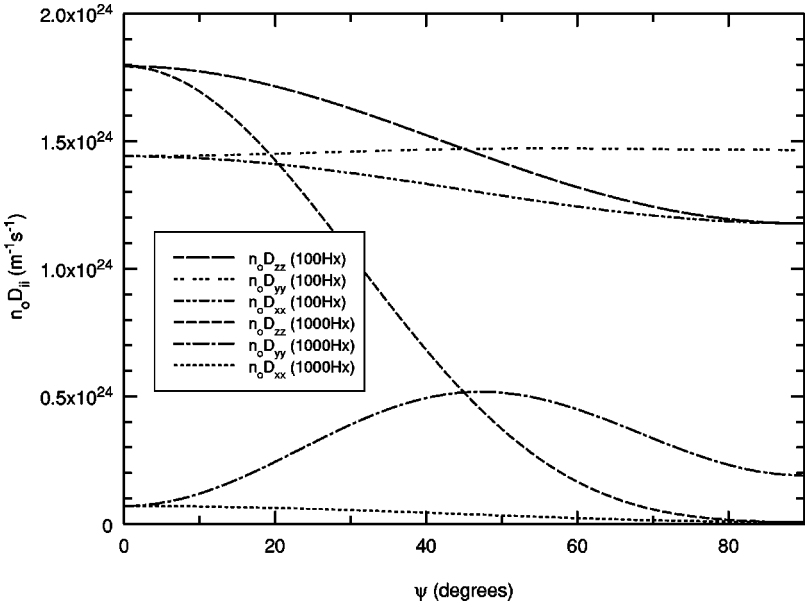

FIG. 3. Variation of the diagonal components of the diffusion tensor as a function of ψ for the Maxwell model (A1).

$$\mathbf{D}=\left\{\mathbf{I}\cdot-\left[1+\left(\frac{\Omega_\mu}{\nu_m}\right)^2\right]^{-1}\left(\left(\frac{\Omega_\mu}{\nu_m}\right)\hat{\boldsymbol{B}}\times-\left(\frac{\Omega_\mu}{\nu_m}\right)^2\hat{\boldsymbol{B}}\times\hat{\boldsymbol{B}}\times\right)\right\}\left(\frac{k\mathbf{T}}{\mu\nu_m}+\frac{\nu_m'}{\nu_m}\boldsymbol{W}\boldsymbol{\gamma}\right), \tag{61}$$

where ν_m' is the energy derivative of ν_m, both of which are averaged over all swarm particles. In this formula, $\Omega_\mu = qB/\mu$ is the gyrofrequency of the charged particles in the center of mass frame, μ is the reduced mass and $\hat{\boldsymbol{B}}$ represents a unit vector in the $\boldsymbol{B}$ direction. In the following we will initially discuss the individual contributions and influences with particular emphasis on their influence on the anisotropic nature of the diffusion tensor. The various couplings will then be addressed.

1. Magnetic anisotropy

For the Maxwell model [Eq. (A1)] and light ion or electron swarms, the thermal contribution is essentially isotropic (to the order of the mass ratio) and the differential velocity effect is absent by virtue of the energy independent collision frequency [32,35]. This model thus enables the anisotropy introduced by explicit orbital effects ($\boldsymbol{B}$ anisotropy) to be isolated and is discussed in the following subsections.

(i) Diagonal elements of the diffusion tensor. The sole effect of magnetic anisotropy in the diffusion tensor is displayed in Fig. 3. Consider initially the parallel field configuration. Diffusion is isotropic in the plane perpendicular to $\boldsymbol{B}$ (i.e., $D_{xx}=D_{yy}$) in accordance with the symmetry properties observed in Sec. II. These coefficients are less than the diffusion coefficient D_{zz}. This represents an example of the $\boldsymbol{B}$ anisotropy of the diffusion tensor. For parallel fields D_{zz} is independent of B/n_o while D_{xx} and D_{yy} monotonically decrease with B/n_o. These effects are gas independent. Indeed, for this model, diffusion is isotropic in the plane perpendicular to $\boldsymbol{B}$ for all ψ (viz., $D_{xx}=D_{zz}$ for $\psi=90°$).

Individually, for a fixed B/n_o, D_{xx}, and D_{zz} are monotonically decreasing functions of ψ, while D_{yy} displays a non-symmetric maximal property with ψ. For a given ψ we observe (again considering additional magnetic fields other than shown) that both D_{xx} and D_{yy} are monotonically decreasing functions of B/n_o, as is D_{zz} provided $\psi\neq 0$.

The variation of the individual elements is due to the variation of the thermal contribution and $\boldsymbol{B}$ anisotropy with ψ. The thermal contribution to diffusion varies with ψ (and B/n_o) in the same manner as that of ε, and hence monotonically decreases with ψ (and B/n_o). To understand qualitatively the explicit effect of $\boldsymbol{B}$ on the diffusion tensor, we recall from the collision free case that the charged particles orbit the magnetic field lines. This explicit orbital effect acts to inhibit diffusion in a plane perpendicular to the magnetic field. It is further strengthened as the magnetic field is increased, since now charged particles complete a greater fraction and number of orbits before undergoing a collision. There is no explicit orbital effect on diffusion parallel to the magnetic field, and diffusion is purely thermal. For D_{zz} the inhibiting explicit orbital effect is strengthened with ψ. The thermal contribution monotonically decreases with ψ, and hence D_{zz} must monotonically decrease with ψ. Conversely, for D_{yy} the variations of thermal and orbital effects with ψ tend to oppose each other, and hence the maximal property with ψ follows. For D_{xx} the explicit orbital effect is constant with ψ, and hence the variation with ψ of D_{xx} follows that of ε. Hence the variation of D_{xx} with ψ is less than that associated with D_{zz}. For all ψ, an increasing magnetic field acts to reduce the thermal contribution and in addition acts to enhance further the inhibiting explicit orbital effect. It then follows that for a given ψ, all the diagonal diffusion coefficients are monotonically decreasing functions of B/n_o. Variations from these trends will be due to the thermal and electric anisotropy discussed in Secs. III C 2 and III C 3.

(ii) Off-diagonal elements of the diffusion tensor. We retain the Maxwell model, to isolate the influence of the magnetic field on the structure of the diffusion tensor with ψ.

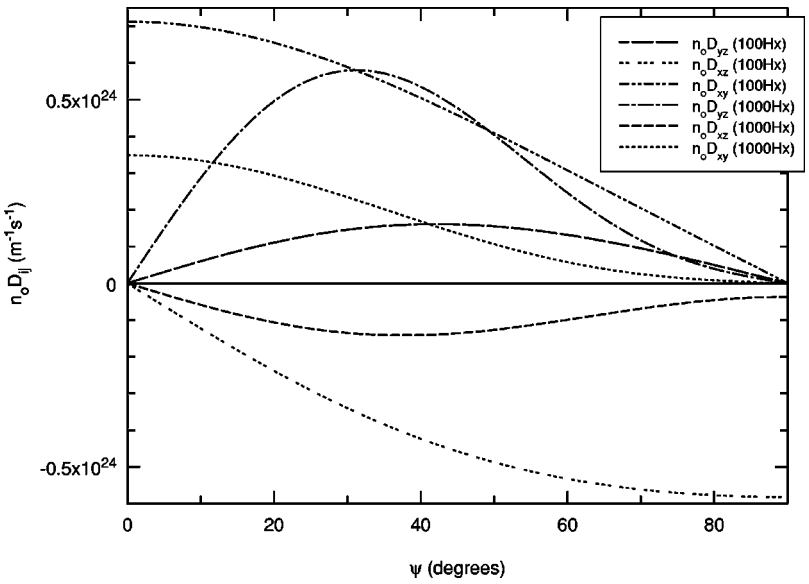

FIG. 4. Variation of the off-diagonal elements of the diffusion tensor as a function of ψ for the Maxwell model (A1).

Specifically for the Maxwell model we note for all ψ (correct to the order of the mass ratio m/m_o) that

$$D_{xy}=-D_{yx}, \quad D_{xz}=-D_{zx}, \quad D_{yz}=D_{zy}, \tag{62}$$

and hence for clarity in Fig. 4 we display only half the off-diagonal components. As Fig. 4 confirms, the off-diagonal components of the diffusion tensor satisfy the symmetry properties outlined in Sec. II, quite generally and independent of the gas considered.

Physically, the off-diagonal elements of the diffusion tensor D_{ij} $(i\neq j)$ appear in relation to a flux in the i direction caused by a density gradient in the j direction. The effects may be generally categorized as Hall currents, familiar in the plasma literature, but we feel that a more detailed discussion is warranted. For this model, the dominant contribution to the off-diagonal elements, at least for this model, arises from the interaction of the gradient-induced fluxes with the magnetic field. Using this interpretation, the general symmetry properties discussed in Sec. II in the limiting cases of parallel and orthogonal fields follow. Consider for example parallel fields. A density gradient in the x direction (suppressing the sign of fluxes at present) will cause a diffusive flux in the x direction. This flux will interact with the magnetic field to cause a flux in the y direction. This flux could then interact with the magnetic field to again produce a flux in the x direction. That is, a gradient in the x direction can cause only a flux in the x (described by D_{xx}) or y direction (described by D_{yx}), but not one in the z direction. Hence the coefficient D_{zx} is zero. Similar arguments can be used to verify the other zero elements of the diffusion tensor. The physical interpretation of negative off-diagonal elements of the diffusion tensor is afforded by considering signs in the above arguments.

The actual variations and magnitudes of the off-diagonal elements are gas dependent. The signs of each will vary according to the magnitude of the influences described below.

2. Thermal anisotropy

The temperature tensor itself is symmetric, in general full and its components satisfy the symmetry properties outlined in Sec. II independent of the gas considered (see Table VI in Appendix B, for example). The diagonal elements of the temperature tensor generally decrease with ψ and B/n_o indicative of the cooling action associated with an increasing perpendicular (to $\boldsymbol{E}$) component of $\boldsymbol{B}$. The variation of the charged-particle temperature with ψ and B/n_o was alluded to previously, and is qualitatively the same as that of the mean energy, independent of the gas. In this section, however, we are primarily interested in the anisotropic nature of the temperature tensor which ultimately influences the anisotropic nature of the diffusion tensor. We note also this anisotropy in the temperature tensor reflects the anisotropy of the distribution function in velocity space and a knowledge of its variation will help interpret the convergence properties dealt with in Sec. III D. Significant inelastic processes are in general required to generate significant anisotropy in the temperature tensor for light ion swarms and for this reason we employ the Reid model (B1). The variation of the anisotropy of the temperature tensor with ψ is displayed in Fig. 5. For parallel fields, we observe the existence of significant anisotropy in the x-z and y-z planes in velocity space. As expected, isotropy exists in the x-y plane for this configuration. As ψ is increased the isotropy in the x-y plane is destroyed. Conversely, increasing ψ acts to reduce the anisotropy in the planes containing the z axis. Any structure beyond this appears to be dependent on the gas considered. The nonmonotonicity of certain ratios is indicative of cooling of the swarm to below the inelastic threshold.

3. Electric anisotropy, gradient energy parameter

Electric anisotropy in the diffusion tensor results from an energy dependent collision frequency and spatial variation of the average energy throughout the swarm. These produce differences in the average ''local'' velocities for a given direction which act to inhibit and/or enhance diffusion in that direction (differential velocity effect). The reader is referred to Refs. [32,35] for a detailed discussion. An example of $\boldsymbol{E}$ anisotropy is evident in Table V for parallel fields at $B/n_o = 50$ Hx. We observe the relation $D_{xx,yy}>D_{zz}$ occurs in spite of the obvious inhibiting orbital effects in the x-y plane and the fact that $T_{xx,yy}<T_{zz}$. The isolated effect of electric anisotropy on the diffusion tensor is described by the term

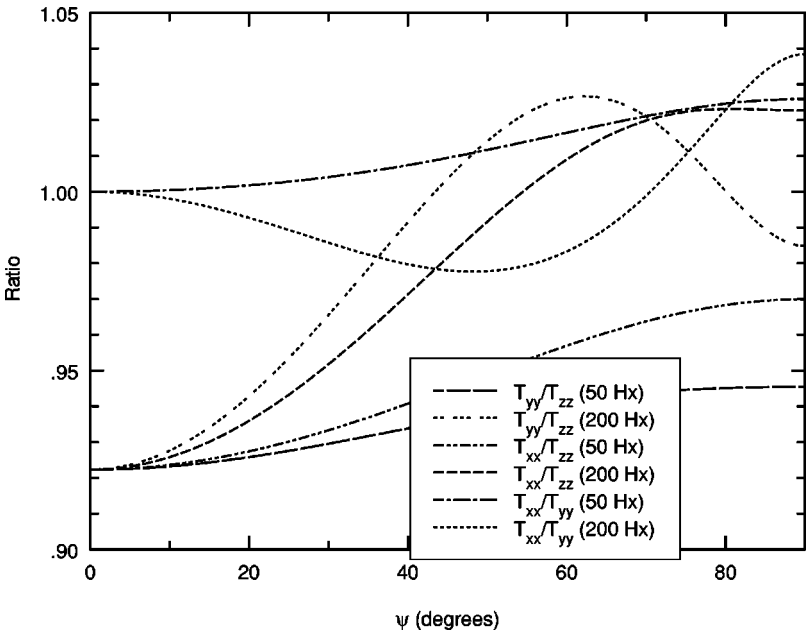

FIG. 5. Variation in the anisotropy of the temperature tensor as a function of ψ for the Reid ramp model (B1).

$\nu_m' W\gamma/\nu_m$ in Eq. (61). A subsequent understanding of variation of the electric anisotropy with ψ is dependent on a knowledge of the variation of the drift velocity components and the gradient energy components with ψ, among other things.

The gradient energy vector γ satisfies the symmetry conditions outlined in Sec. II ($\gamma_x=\gamma_y=0$ for $\psi=0$, while $\gamma_y=0$ for $\psi=90°$), independent of the gas considered. For light ion swarms undergoing predominantly elastic interactions, first order spatial variation is predominant only in the y and z directions (see, e.g., Table II in Appendix A). There is very little spatial variation in the average energy in the $\boldsymbol{E}\times\boldsymbol{B}$ direction. It appears that significant inelastic processes are required to establish appreciable spatial variation of the average energy in this direction (see, e.g., Table IV in Appendix B). Importantly, we note that γ_y and γ_z are negative (or zero) for all ψ, indicating the average energy increases through the swarm in these directions in the direction that the swarm is drifting. The latter result follows from the fact that on average the charged particles at the front of the swarm in the z direction have fallen through a greater potential difference and should be more energetic. Conversely, we observe for the Reid model that the spatial variation in the average energy in the $\boldsymbol{E}\times\boldsymbol{B}$-direction is in the opposite direction to the drift in that direction. This has important ramifications for weak fields (viz. $B/n_o=50$ Hx) where D_{xx} actually increases with ψ. The magnitudes of γ_y and γ_z display a maximal property and monotonically, decrease respectively, with ψ. The latter results from the reduction in the ability of the electric field to efficiently input energy as ψ is increased.

4. Couplings of the anisotropies

The anisotropic nature of the diffusion tensor resulting from the combined effects of all of sources of anisotropy is

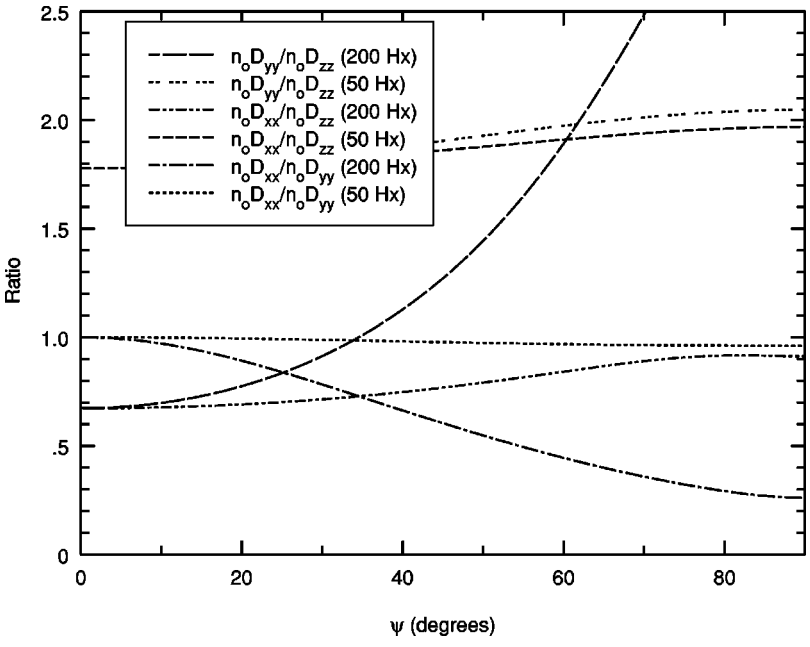

FIG. 6. Variation in the anisotropy of the diffusion tensor as a function of ψ for the Reid ramp model (B1).

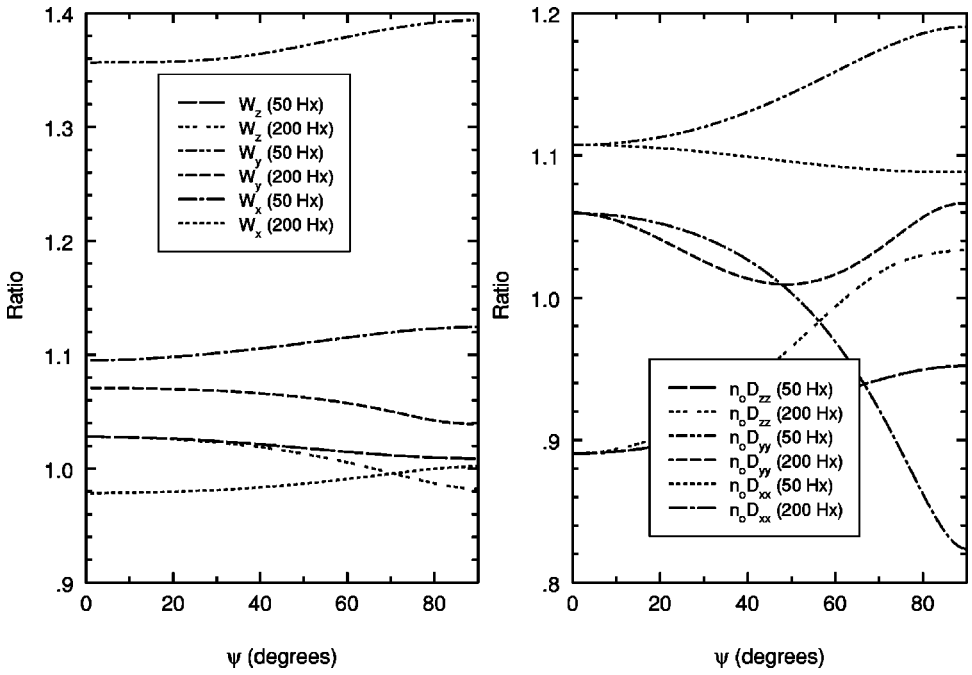

FIG. 7. Comparison of the ratio of the two-term and multiterm values for the drift velocity components and diagonal diffusion tensor elements as a function of ψ for the Reid ramp model (B1).

demonstrated in Fig. 6 using the Reid ramp model (B1). Up to now we have discussed the individual contributions to or influences on the diffusion tensor and its anisotropic nature. The variation of these contributions and influences with ψ and B/n_o is complex, with both explicit (i.e., due to the field configuration) and implicit (due to the variation in the mean energy and hence the collisional processes) variations. Further complexity is added by virtue of the couplings between the magnetic and thermal anisotropies and the magnetic and electric anisotropies as is indicated by the action of the operators in $\{\}$ on the thermal and differential velocity terms in $(\,)$ of Eq. (61). One can observe from this equation that the element D_{ij} is not only dependent on the direct contributions and influences T_{ij} and $W_i\gamma_j$, but also the indirect contributions and influences T_{kj} and $W_k\gamma_j$ where $k=x,y,z\neq i$. These indirect processes arise from the various order rotations of motion due to the Lorentz force (viz. the first operator in $\{\}$ is the direct component, the second is due to first order rotations which produce an effective motion in the i direction, and, the last operator represents second order rotations which influence motion in the i direction). The rotations of various orders are also weighted according to the gyro to collision frequency ratio. Although one can generalize the above arguments to incorporate such rotations, we find it sufficient here to highlight these contributing processes and their couplings without recourse to detailed and cumbersome comparisons of these individual processes associated with each element of the tensor.

D. Two-term vs multiterm approximations; validity of Legendre polynomial expansions

The convergence of the spherical harmonics expansion is dependent on the dominant types of collisional processes present. In general for gases with elastic collisional processes, as with the electric field only case, the two-term approximation [viz. the truncation of Eq. (2) to $l_{\max}=1$] is sufficient to ensure accuracies of the order of 2% or less. *It is the exception, however, more than the rule, that the two-term approximation is sufficient.* To this end, we explore the Reid ramp model due to the known failure of the two-term approximation in the electric field only case. In Fig. 7, we display the ratios of the two-term and multiterm values for the drift velocity and diagonal diffusion tensor components. The inadequacy of the two-term approximation for all transport coefficients and properties for this model is clearly evident. In particular the errors associated with the off-diagonal elements of the (symmetric part of the) diffusion tensor are noteworthy and are of the order of 200% (see Table VII in Appendix B). The drift velocity and diagonal diffusion tensor components can have errors of the order of 40% and 20%, respectively. For transport parallel to $\boldsymbol{E}$ the error associated with the two-term approximation is generally reduced with increasing ψ. This appears to reflect the general trend to reduce anisotropy of the velocity distribution function in the z direction as ψ increases, as discussed previously. In contrast, for transport perpendicular to $\boldsymbol{E}$, it appears in general that errors associated with the two-term approximation are enhanced with increasing ψ, reflecting the enhancement of the anisotropy of the velocity distribution in the planes perpendicular to $\boldsymbol{E}$, as detailed above. This appears to contradict the general trend predicted in the $\boldsymbol{E}$-only case, where a reduction in the mean energy (here associated with an increasing ψ) acts to reduce the effect of the inelastic processes causing the anisotropy. Thus estimates of the accuracy of the two-term approximation based on the $\boldsymbol{E}$-only case can be misleading when applied to the present system. It should also be highlighted that a smaller error in the two term approximation does not necessarily ensure quicker convergence in the l-index and vice-versa (viz. W_x for $B/n_o=50$ Hx in Table VII).

The consideration of the m dependence of the velocity distribution function is, aside from an intrinsic interest, important from a computational standpoint. Our ability to truncate the m summation dramatically reduces the matrix size and hence decreases the computation time. In Table VIII,

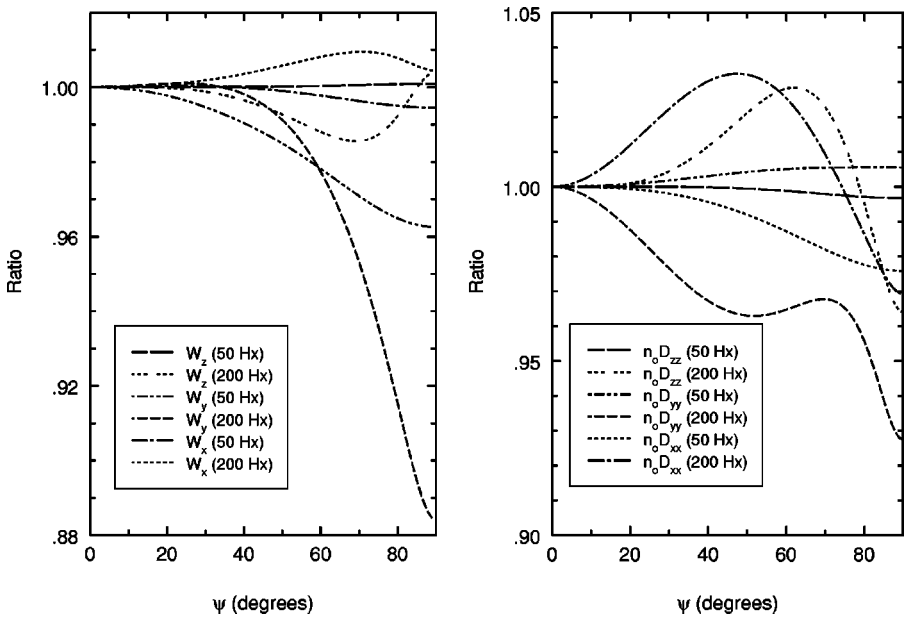

FIG. 8. Comparison of the ratio of the $m_{\max}=1$ and 5 truncations ($l_{\max}=5$) for the drift velocity components and diagonal elements of the diffusion tensor as a function of ψ for the Reid ramp model (B1).

convergence of the transport coefficients and properties in the m-index is displayed. A value of $l_{\max}=5$ was chosen, and the m index was incremented up to $l_{\max}$. A value of $m_{\max}=0$ represents a Legendre polynomial expansion (with its principal axis in the $\boldsymbol{E}$ direction). The Legendre polynomial expansion is inadequate for determining transport perpendicular to $\boldsymbol{E}$. For parallel fields, as expected the Legendre polynomial expansion is sufficient to determine transport parallel to the electric field, this being an axis of symmetry. However, convergence in the m index is rapid for parallel fields with $m_{\max}=1$ sufficient to achieve 0.1% accuracy for all transport coefficients and properties. For low B/n_o, $m_{\max}=2$ is sufficient to generate errors of less than 0.5% for all transport properties at all ψ. The coefficient D_1 appears most sensitive to the m truncation. In Fig. 8, the ratio of the results for $m_{\max}=1$ and $m_{\max}=5$ for a six-term approximation are given for the drift velocity and diagonal diffusion tensor components. For low B/n_o, it can be seen that the m dependence is increased with increasing ψ. For high B/n_o the m dependence generally displays some maximal property with ψ. This result reflects the reduction in the l dependence as ψ is increased. We note also, through consideration of more B/n_o than shown, that the initial m dependence is in general strengthened as B/n_o is increased.

IV. CONCLUDING REMARKS

In this work we have presented, first, a formal theoretical analysis of charged-particle transport in gases under the influence of spatially homogeneous electric and magnetic fields crossed at arbitrary angles (ψ) to each other using a multiterm solution of the Boltzmann equation. The structure of the tensors associated with the transport properties was addressed through symmetry considerations. Second, we have presented numerical results for light ions and electron swarms and addressed physical explanations for the variation of the transport properties and coefficients with ψ for various B/n_o. In particular we have discussed the ''triple anisotropy'' phenomenon of the diffusion tensor arising from $\boldsymbol{E}$, $\boldsymbol{B}$, and thermal effects. Benchmark results are given in Appendixes A and B for the Maxwell and Reid ramp models. Comparison with analytic values and/or previous theories have shown our numerical calculations are of high accuracy. In this work we displayed and emphasized the need for a multiterm solution technique and highlighted the inability of a Legendre polynomial expansion to accurately represent the entire velocity distribution function. An important observation is that indications of the soundness or otherwise of the two-term approximations based on $\boldsymbol{E}$-only results do not necessarily carry over to the case where $\boldsymbol{B}$ is also present. We have also investigated the correlation of the convergence in the l and m indices with ψ and B/n_o. These correlations have been further investigated through comparisons with calculated velocity distribution functions for swarms in $\boldsymbol{E}$ and $\boldsymbol{B}$ fields at various ψ [40]. We should emphasize here that although we have restricted our discussions here to light charged-particle swarms, the theory developed here, based on an expansion about a ''multi-Maxwellian'' weighting function, is equally valid for ion swarms.

In the presence of reactions it is well known that the transport coefficients are modified due to the transport brought about by nonuniform creation or annihilation of swarm particles (see, e.g. Ref. [36]). One must go to second order in the density gradient expansion (3) to account accurately for such effects. Ness and Makabe [37] recently considered such effects for crossed electric and magnetic fields. The generalization to arbitrary configurations remains the focus of future investigations.

ACKNOWLEDGMENTS

Our special thanks go to Dr. Stephen Biagi for his useful discussions and for making the results of his Monte Carlo simulations available to us prior to publication. We wish to also acknowledge the financial support of the Australian Re-

TABLE II. Average energy properties and drift velocity components as a function of the angle between $\boldsymbol{E}$ and $\boldsymbol{B}$ for the Maxwell model. The numbers in parentheses are the analytic values based on the assumption of an isotropic temperature tensor. ($E/n_o = 1$ Td, $B/n_o = 1000$ Hx, $T_o = 293$ K, and $m_o = 4$ amu.)

Transport coefficient or property	ψ				
	0°	30°	45°	60°	90°
ε	0.54430	0.42267	0.30104	0.17942	0.057787
(eV)	(0.54423)	(0.42262)	(0.30101)	(0.17940)	(0.057787)
W_x	0	−0.48034	−0.67930	−0.83197	−0.96068
(10^3 ms^{-1})	(0)	(−0.48034)	(−0.67930)	(−0.83197)	(−0.96067)
W_y	0	2.0561	2.3742	2.0561	0
(10^3 ms^{-1})	(0)	(2.0560)	(2.3741)	(2.0560)	(0)
W_z	4.9428	3.7557	2.5686	1.3815	0.19436
(10^3 ms^{-1})	(4.9425)	(3.7554)	(2.5684)	(1.3814)	(0.19437)
$n_o\gamma_x$	0	1.3847×10^{-4}	1.3169×10^{-4}	8.2742×10^{-5}	4.8419×10^{-6}
(kg s^2)	(0)	(0)	(0)	(0)	(0)
$n_o\gamma_y$	0	−19.030	−15.650	−8.0771	0
(kg s^2)	0	(−19.017)	(−15.640)	(−8.0724)	(0)
$n_o\gamma_z$	−58.910	−34.758	−16.930	−5.4261	−0.24580
(kg s^2)	(−58.870)	(−34.736)	(−16.920)	(−5.4237)	(−0.24582)

search Council and the High Performance Computing Center at James Cook University.

APPENDIX A: BENCHMARK RESULTS: MAXWELL MODEL

In this appendix we present benchmark results for future calculations of the following Maxwell model (constant collision frequency model):

$$\sigma_m(\epsilon) = 6\epsilon^{-1/2}\ \text{Å}^2\ \text{(elastic cross section)},$$

$$m_o = 4\ \text{amu},\quad m = 5.486\times10^{-4}\ \text{amu},\quad T_o = 293\ \text{K},$$

$$E/n_o = 1\ \text{Td},$$

$$q = +e, \tag{A1}$$

where ϵ is in eV and e is the electronic charge. For this model the Boltzmann equation can be solved exactly, and analytic expressions obtained for the transport properties. Further simplification results if $\mathbf{T}$ is assumed to be isotropic.

TABLE III. Diffusion tensor components as a function of the angle between $\boldsymbol{E}$ and $\boldsymbol{B}$ for the Maxwell model. The numbers in parentheses are the analytic values based on the assumption of an isotropic temperature tensor. ($E/n_o = 1$ Td, $B/n_o = 1000$ Hx, $T_o = 293$ K, and $m_o = 4$ amu.)

Transport coefficient or property	ψ				
	0°	30°	45°	60°	90°
n_oD_{xx}	0.70508	0.54753	0.38998	0.23242	0.074872
(10^{23} m^{-1} s^{-1})	(0.70522)	(0.54763)	(0.39005)	(0.23246)	(0.074880)
n_oD_{yy}	0.70508	3.8931	5.1556	4.4926	1.9040
(10^{23} m^{-1} s^{-1})	(0.70522)	(3.8920)	(5.1541)	(4.4915)	(1.9041)
n_oD_{zz}	17.938	10.584	5.1555	1.6524	0.074876
(10^{23} m^{-1} s^{-1})	(17.932)	(10.581)	(5.1541)	(1.6521)	(0.074880)
n_oD_{xy}	3.4851	2.3438	1.3630	0.57446	0
(10^{23} m^{-1} s^{-1})	(3.4855)	(2.3440)	(1.3632)	(0.57448)	(0)
n_oD_{yx}	−0.38451	−2.3438	−1.3631	−0.57445	0
(10^{23} m^{-1} s^{-1})	(−0.38455)	(−2.3440)	(−1.3632)	(−0.57448)	(0)
n_oD_{xz}	0	−1.3532	−1.3630	−0.99491	−0.37009
(10^{23} m^{-1} s^{-1})	(0)	(−1.3533)	(−1.3662)	(−0.99502)	(−0.37009)
n_oD_{zx}	0	1.3531	1.3630	0.99490	0.37009
(10^{23} m^{-1} s^{-1})	(0)	(1.3533)	(1.3662)	(0.99502)	(0.37009)
n_oD_{yz}	0	5.7946	4.7655	2.4595	0
(10^{23} m^{-1} s^{-1})	(0)	(5.7927)	(4.7641)	(2.4589)	(0)
n_oD_{zy}	0	5.7947	4.7656	2.4596	0
(10^{23} m^{-1} s^{-1})	(0)	(5.7927)	(4.7641)	(2.4589)	(0)

TABLE IV. Average energy properties and drift velocity components as a function of the angle between $\boldsymbol{E}$ and $\boldsymbol{B}$ for the Reid ramp model (B1) ($E/n_o = 12$ Td).

Transport coefficient or property	B/n_o (Hx)	ψ 0°	30°	45°	60°	90°
ε (eV)	50	0.2689	0.2673	0.2655	0.2636	0.2616
	200	0.2689	0.2569	0.2418	0.2212	0.1816
$W_x(10^4\ \mathrm{m\ s^{-1}})$	50	0	−0.9559	−1.374	−1.714	−2.020
	200	0	−1.699	−2.517	−3.277	−4.208
$W_y(10^4\ \mathrm{m\ s^{-1}})$	50	0	0.2654	0.3164	0.2840	0
	200	0	1.872	2.423	2.465	0
$W_z(10^4\ \mathrm{m\ s^{-1}})$	50	6.838	6.737	6.632	6.520	6.401
	200	6.838	6.109	5.253	4.186	2.573
$n_o\gamma_x(10^{-1}\ \mathrm{kg\ s^2})$	50	0	−0.1336	−0.2057	−0.2777	−0.3611
	200	0	−0.1348	−0.2221	−0.3420	−0.7385
$n_o\gamma_y(10^{-1}\ \mathrm{kg\ s^2})$	50	0	−0.1469	−0.1755	−0.1580	0
	200	0	−1.064	−1.464	−1.673	0
$n_o\gamma_z(10^{-1}\ \mathrm{kg\ s^2})$	50	−3.666	−3.640	−3.615	−3.592	−3.573
	200	−3.666	−3.414	−3.131	−2.814	−2.634

In Tables II and III, the results of the present Boltzmann solution are compared with the analytic values for a range of ψ. Convergence in both the l and ν indices is excellent for this model. We found $l_{\max}=2$ was sufficient to ensure five figure accuracy. For orthogonal fields the results are in excellent agreement with Ness [25] and Monte Carlo simulations of Ref. [34]. Agreement to at least 1% exists between the calculated and analytic values for all transport coefficients, and for all angles. The discrepancies in the results are attributable to the approximation of an isotropic temperature tensor in the analytic values. The implications for such an assumption for this model are evident in certain analytic results, e.g., $|D_{ij}|=|D_{ji}|$ for $i\neq j$. We emphasize here that in general the temperature tensor is not isotropic and is in fact full, aside from the limits of parallel and orthogonal fields, in which the symmetry properties discussed previously are satisfied.

APPENDIX B: BENCHMARK RESULTS: REID RAMP MODEL

The Reid ramp model [33] has been used extensively as a benchmark for a variety of field combinations, profiles, and configurations [24,25,32,38] due to its well known illustration of the failure of the two term approximation. In this appendix we extend the model to consider static electric and magnetic fields at arbitrary angles to each other. The details of the model are:

TABLE V. Diffusion tensor components as a function of the angle between $\boldsymbol{E}$ and $\boldsymbol{B}$ for the Reid ramp model (B1) ($E/n_o = 12$ Td).

Transport coefficient or property	B/n_o (Hx)	ψ 0°	30°	45°	60°	90°
$n_oD_{xx}[10^{24}(\mathrm{m\ s})^{-1}]$	50	1.011	1.026	1.044	1.065	1.093
	200	0.3827	0.3694	0.3526	0.3296	0.2950
$n_oD_{yy}[10^{24}(\mathrm{m\ s})^{-1}]$	50	1.011	1.039	1.068	1.101	1.137
	200	0.3827	0.4722	0.5838	0.7412	1.129
$n_oD_{zz}[10^{24}(\mathrm{m\ s})^{-1}]$	50	0.5689	0.5648	0.5610	0.5578	0.5554
	200	0.5689	0.5173	0.4592	0.3918	0.3233
$n_oD_{xy}[10^{24}(\mathrm{m\ s})^{-1}]$	50	0.356	0.3153	0.2642	0.1923	0
	200	0.5282	0.4805	0.4195	0.3311	0
$n_oD_{yx}[10^{24}(\mathrm{m\ s})^{-1}]$	50	−0.356	−0.3194	−0.2722	−0.2025	0
	200	−0.5282	−0.4730	−0.4048	−0.3098	0
$n_oD_{xz}[10^{24}(\mathrm{m\ s})^{-1}]$	50	0	−0.03586	−0.04836	−0.05545	−0.05798
	200	0	−0.1499	−0.2111	−0.2530	−0.2491
$n_oD_{zx}[10^{24}(\mathrm{m\ s})^{-1}]$	50	0	0.1296	0.1881	0.2374	0.2847
	200	0	0.2238	0.3196	0.3957	0.4676
$n_oD_{yz}[10^{24}(\mathrm{m\ s})^{-1}]$	50	0	−0.00193	−0.00372	−0.00495	0
	200	0	0.06833	0.07682	0.05663	0
$n_oD_{zy}[10^{24}(\mathrm{m\ s})^{-1}]$	50	0	0.03442	0.04135	0.03747	0
	200	0	0.2022	0.2686	0.2878	0

TABLE VI. The elements of the temperature tensor as a function of the angle between $\boldsymbol{E}$ and $\boldsymbol{B}$ for the Reid ramp model (B1). ($E/n_o = 12$ Td.)

Element	B/n_o (Hx)	ψ 0°	30°	45°	60°	90°
$T_{xx}(10^3\ \mathrm{K})$	50	1.924	1.923	1.922	1.921	1.921
	200	1.924	1.851	1.759	1.632	1.378
$T_{yy}(10^3\ \mathrm{K})$	50	1.924	1.915	1.904	1.890	1.872
	200	1.924	1.878	1.799	1.659	1.327
$T_{zz}(10^3\ \mathrm{K})$	50	2.086	2.060	2.034	2.007	1.980
	200	2.086	1.945	1.792	1.617	1.348
T_{xy}(K)	50	0	−4.767	−8.325	−9.525	0
	200	0	−15.57	−28.23	−34.09	0
T_{xz}(K)	50	0	−36.78	−49.66	−57.54	−61.95
	200	0	−29.56	−30.96	−21.36	1.925
T_{yz}(K)	50	0	14.95	16.39	13.27	0
	200	0	58.54	51.19	22.01	0
$T_e(10^3\ \mathrm{K})$	50	1.978	1.966	1.953	1.940	1.924
	200	1.978	1.891	1.783	1.636	1.351

TABLE VII. Convergence in the l index for various transport coefficients and properties as a function of the angle between $\boldsymbol{E}$ and $\boldsymbol{B}$ for the Reid ramp model (B1) ($E/n_o = 12$ Td, $B/n_o = 50$ Hx).

Transport coefficient or property	ψ (deg)	$l_{\max}$ 1	2	3	4	5	6
ε (eV)	0	0.27359	0.26894	0.26885	0.26898	0.26893	0.26894
	45	0.26866	0.26557	0.26553	0.26551	0.26551	0.26551
	90	0.26277	0.26160	0.26158	0.26156	0.26156	0.26155
$W_x(10^4\ \mathrm{m\,s^{-1}})$	0	0	0	0	0	0	0
	45	−1.5222	−1.3709	−1.3735	−1.3742	−1.3741	−1.3742
	90	−2.2707	−2.0206	−2.0203	−2.0198	−2.0200	−2.0201
$W_y(10^4\ \mathrm{m\,s^{-1}})$	0	0	0	0	0	0	0
	45	0.43276	0.31249	0.31394	0.31617	0.31653	0.31632
	90	0	0	0	0	0	0
$W_z(10^4\ \mathrm{m\,s^{-1}})$	0	7.0296	6.8207	6.8411	6.8372	6.8386	6.8381
	45	6.7622	6.6228	6.6323	6.6318	6.6316	6.6317
	90	6.4582	6.3962	6.3998	6.4011	6.4009	6.4009
$n_o D_{xx}[10^{24}(\mathrm{m\,s})^{-1}]$	0	1.1196	1.0146	1.0080	1.0123	1.0111	1.0113
	45	1.1456	1.0494	1.0429	1.0436	1.0438	1.0438
	90	1.1891	1.1108	1.0937	1.0928	1.0928	1.0928
$n_o D_{yy}[10^{24}(\mathrm{m\,s})^{-1}]$	0	1.1196	1.0146	1.0080	1.0123	1.0111	1.0113
	45	1.2142	1.0578	1.0698	1.0678	1.0682	1.0682
	90	1.3533	1.1296	1.1366	1.1368	1.1368	1.1368
$n_o D_{zz}[10^{24}(\mathrm{m\,s})^{-1}]$	0	0.50653	0.57398	0.56841	0.56904	0.56882	0.56890
	45	0.51422	0.56307	0.56088	0.56100	0.56104	0.56102
	90	0.52876	0.55636	0.55558	0.55533	0.55536	0.55535
$n_o D_1[10^{23}(\mathrm{m\,s})^{-1}]$	0	0	0	0	0	0	0
	45	0.14192	−0.1879	−0.0810	−0.0714	−0.0803	−0.0795
	90	0	0	0	0	0	0
$n_o D_2[10^{22}(\mathrm{m\,s})^{-1}]$	0	0	0	0	0	0	0
	45	26.441	13.283	13.959	13.957	13.972	13.971
	90	41.915	22.707	22.766	22.664	22.667	22.671
$n_o D_3[10^{22}(\mathrm{m\,s})^{-1}]$	0	0	0	0	0	0	0
	45	1.930	3.964	3.771	3.775	3.758	3.763
	90	0	0	0	0	0	0

TABLE VIII. Convergence in the m index for various transport coefficients and properties as a function of the angle between $\boldsymbol{E}$ and $\boldsymbol{B}$ for the Reid ramp model (B1) ($E/n_o = 12$ Td, $B/n_o = 50$ Hx, and $l_{\max} = 5$ throughout).

Transport coefficient or property	ψ (deg)	$m_{\max}$ 0	1	2	3	4	5
ε (eV)	0	0.26893	0.26893	0.26893	0.26893	0.26893	0.026893
	45	0.26893	0.2655	0.2655	0.2655	0.2655	0.2655
	90	0.26893	0.2617	0.2616	0.2616	0.2616	0.2616
$W_x(10^4\ \mathrm{m\,s^{-1}})$	0	0	0	0	0	0	0
	45	0	−1.373	−1.374	−1.374	−1.374	−1.374
	90	0	−2.009	−2.020	−2.020	−2.020	−2.020
$W_y(10^4\ \mathrm{m\,s^{-1}})$	0	0	0	0	0	0	0
	45	0	0.3126	0.3165	0.3166	0.3165	0.3165
	90	0	0	0	0	0	0
$W_z(10^4\ \mathrm{m\,s^{-1}})$	0	6.839	6.839	6.839	6.839	6.839	6.839
	45	6.389	6.632	6.632	6.632	6.632	6.632
	90	6.839	6.407	6.401	6.401	6.401	6.401
$n_oD_{xx}[10^{24}(\mathrm{m\,s})^{-1}]$	0	0	1.011	1.011	1.011	1.011	1.011
	45	0	1.038	1.044	1.044	1.044	1.044
	90	0	1.066	1.092	1.093	1.093	1.093
$n_oD_{yy}[10^{24}(\mathrm{m\,s})^{-1}]$	0	0	1.011	1.011	1.011	1.011	1.011
	45	0	1.072	1.068	1.068	1.068	1.068
	90	0	1.143	1.136	1.137	1.137	1.137
$n_oD_{zz}[10^{24}(\mathrm{m\,s})^{-1}]$	0	0.5688	0.5688	0.5688	0.5688	0.5688	0.5688
	45	0.5688	0.5609	0.5610	0.5610	0.5610	0.5610
	90	0.5688	0.5536	0.5552	0.5554	0.5554	0.5554
$n_oD_1[10^{22}(\mathrm{m\,s})^{-1}]$	0	0	0	0	0	0	0
	45	0	0.476	−0.790	−0.809	−0.802	−0.803
	90	0	0	0	0	0	0
$n_oD_2[10^{22}(\mathrm{m\,s})^{-1}]$	0	0	0	0	0	0	0
	45	0	13.71	13.97	13.97	13.97	13.97
	90	0	21.07	22.60	22.67	22.67	22.67
$n_oD_3[10^{22}(\mathrm{m\,s})^{-1}]$	0	0	0	0	0	0	0
	45	0	3.907	3.759	3.756	3.758	3.758
	90	0	0	0	0	0	0

$$\sigma_0^{\mathrm{inel}}(\epsilon) = \begin{cases} 10(\epsilon - 0.2)\ \text{Å}^2, & \epsilon \geqslant 0.2\ \text{eV (total inelastic cross section)} \\ 0, & \epsilon < 0.2\ \text{eV}, \end{cases}$$

$$\sigma_0^{\mathrm{elast}}(\epsilon) = 6\ \text{Å}^2 \quad \text{(total elastic cross section)},$$

$$m_o = 4\ \text{amu}, \quad m = 5.486 \times 10^{-4}\ \text{amu}, \quad T_o = 0\ \text{K}; \quad q = +e,$$

$$E/n_o = 12\ \text{Td}. \tag{B1}$$

Scattering for this model is isotropic.

The results for this model are displayed in Tables IV–VI. For orthogonal fields, the results are in excellent agreement with those of Ness [25] and Ref. [34]. For parallel fields, the values of ε, W_z, and D_{zz} are also in excellent agreement with those associated with a pure static dc electric field [24,33], while, as expected, the values of D_{xx} and D_{yy} differ substantially from D_T in the electric field only case. These ''benchmarks'' support the numerical integrity of the present theory and code. In Table VII we investigate the convergence of the transport properties in the l index. Convergence in the m index is displayed in Table VIII, where $l_{\max} = 5$ is fixed.

[1] M. J. Liebermann and A. J. Lichtenberg, *Principles of Plasma Discharges and Materials Processing* (Wiley, New York, 1994).
[2] B. Schwarzchild, Phys. Today **6** (1), 17 (1993).
[3] R. W. Crompton, Adv. At., Mol., Opt. Phys. **32**, 97 (1994).
[4] B. Schmidt, Comments At. Mol. Phys. **28**, 379 (1993); Phys. Scr. **T53**, 30 (1994).
[5] W. M. Pickering and D. W. Windle, Planet. Space Sci. **18**, 1153 (1976); W. Jones, *ibid.* **39**, 1283 (1991).
[6] M. J. Brennan, A. M. Garvie, and L. J. Kelly, Aust. J. Phys. **43**, 27 (1990).
[7] K. F. Ness, Phys. Rev. A **47**, 327 (1993).
[8] R. E. Robson, Aust. J. Phys. **47**, 279 (1994).
[9] R. Winkler, Plasma Phys. **27**, 317 (1972).
[10] L. G. H. Huxley and R. W. Crompton, *The Diffusion and Drift of Electrons in Gases* (Wiley, New York, 1974).
[11] G. L. Braglia and L. Ferrari, Physica (Amsterdam) **67**, 249 (1973); **67**, 274 (1973).
[12] S. F. Biagi, Nucl. Instrum. Methods Phys. Res. A **273**, 533 (1989); **283**, 716 (1990).
[13] S. F. Biagi, Nucl. Instrum. Methods Phys. Res. A **421**, 234 (1999).
[14] R. E. Robson, M. Hildebrandt, and B. Schmidt, Nucl. Instrum. Methods Phys. Res. A **394**, 74 (1997).
[15] D. C. Kelly, Phys. Rev. **119**, 27 (1960).
[16] I. P. Shkarofsky, T. W. Johnston, and M. P. Bachynski, *The Particle Kinetics of Plasmas* (Addison-Wesley, London, 1966).
[17] E. B. Wagner, F. J. Davis, and G. S. Hurst, J. Chem. Phys. **47**, 3138 (1967).
[18] H. R. Skullerud, J. Phys. B **2**, 696 (1969); R. E. Robson, Aust. J. Phys. **25**, 685 (1972).
[19] W. Blum and L. Rolandi, *Particle Detection with Drift Chambers* (Springer, Berlin, 1993).
[20] B. Li, R. E. Robson, and R. D. White, in *Proceedings of the XXII ICP16 Conference, Toulouse, France, 1997*, edited by M. C. Bordage (Université Paul Sabatier, Toulouse, France, 1997), Vol. 1, p. 52.
[21] N. Ikuta and Y. Sugai, J. Phys. Soc. Jpn. **64**, 1228 (1989).
[22] R. E. Robson, Aust. J. Phys. **48**, 677 (1995); K. Kumar, J. Phys. Soc. Jpn. **64**, 4583 (1995).
[23] L. A. Viehland and E. A. Mason, Ann. Phys. (N.Y.) **91**, 499 (1978).
[24] K. F. Ness and R. E. Robson, Phys. Rev. A **34**, 2185 (1986).
[25] K. F. Ness, J. Phys. D **27**, 1848 (1994).
[26] K. F. Ness and L. A. Viehland, Chem. Phys. **148**, 225 (1990).
[27] L. Boltzmann, Sitzungsber. Akad. Wiss. Wien **66**, 275 (1872) [English translation: S. G. Brush, *Irreversible Processes* (Pergamon, Oxford, 1966), Vol. 2, p. 88].
[28] C. S. Wang-Chang, G. E. Uhlenbeck, and J. De Boer, in *Studies in Statistical Mechanics*, edited by J. De Boer and G. E. Uhlenbeck (Wiley, New York, 1962), Vol. II, p. 241.
[29] L. Viehland, Phys. Scr. **T53**, 53 (1994); K. F. Ness and R. E. Robson, Transp. Theory Stat. Phys. **14**, 257 (1985).
[30] E. A. Mason and E. W. McDaniel, *Transport Properties of Ions in Gases* (Wiley, New York, 1988).
[31] S. L. Lin, R. E. Robson, and E. A. Mason, J. Chem. Phys. **71**, 3483 (1979).
[32] R. D. White, R. E. Robson, and K. F. Ness, Aust. J. Phys. **48**, 925 (1995).
[33] I. Reid, Aust. J. Phys. **32**, 231 (1979).
[34] R. D. White, M. J. Brennan, and K. F. Ness, J. Phys. D **30**, 810 (1997).
[35] R. E. Robson, R. D. White, and T. Makabe, Ann. Phys. (N.Y.) **261**, 74 (1997).
[36] K. Kumar, H. R. Skullerud, and R. E. Robson, Aust. J. Phys. **33**, 343 (1980).
[37] K. F. Ness and T. Makabe (unpublished).
[38] K. Maeda, T. Makabe, N. Nakano, S. Bzenic, and Z. Lj. Petrovic, Phys. Rev. E **55**, 5901 (1997).
[39] R. E. Robson and K. F. Ness, Phys. Rev. E **33**, 2068 (1986).
[40] R. D. White, K. F. Ness, and R. E. Robson (unpublished).